



# Difunctional 1H-quinolin-2-ones as spectroscopic fluorescent probes for real-time monitoring of photopolymerisation process and photosensitizers of fluorescent photopolymer resin in 3D printing

Monika Topa<sup>a</sup>, Filip Petko<sup>b</sup>, Mariusz Galek<sup>b</sup>, Magdalena Jankowska<sup>a</sup>, Roman Popielarz<sup>a</sup>, Joanna Ortyl<sup>a,b,\*</sup>

<sup>a</sup> Department of Biotechnology and Physical Chemistry, Faculty of Chemical Engineering and Technology, Cracow University of Technology, Warszawska 24, 30-155 Kraków, Poland

<sup>b</sup> Photo HiTech Ltd., Bobrzyńskiego 14, 30-348 Cracow, Poland

## ARTICLE INFO

### Keywords:

Fluorescent molecular sensors  
Photopolymerisation  
Fluorescence Probe Technology  
Photosensitizer  
Cationic photopolymerisation  
Free-radical photopolymerisation  
Thiol-ene photopolymerisation  
3D printing

## ABSTRACT

Herein, novel 1H-quinolin-2-ones derivatives dedicated to polymer chemistry have been reported. Essential spectroscopic studies including absorbance, fluorescence emission and excitation spectra were carried out. Subsequently, a number of studies on the suitability of new compounds for the role of fluorescent molecular probes using Fluorescence Probe Technology were performed. The research present also the suitability of these compounds as co-initiators in a two-component system: 1H-quinolin-2-ones/4,4'-dimethyl-diphenyl iodonium hexafluorophosphate (OMNICAT 440). Cationic photopolymerisation processes of CADE epoxy and vinyl TEGDVE monomers, free-radical photopolymerisation of TMPTA acrylic monomer as well as thiol-ene photopolymerisation of a mixture of monomers: TATATO/MERCAPTO when exposed to UV light with maximum emission at 365 nm and visible light with maximum emission at 405 nm were carried out. Finally, the applicability of novel initiating systems to obtain fluorescent 3D prints was introduced.

## 1. Introduction

Ultra-violet and visible light-based polymerisation has several precise advantages [1,2]. Due to its low energy consumption, lack of solvents and the fact that the reaction occurs at ambient temperature, it remains environmentally friendly and harmless [3]. Furthermore, both the photopolymerisation and curing processes are exceptionally rapid and occur within a few seconds [2,4]. A variety of research techniques have been employed to study polymers obtained through photopolymerisation. Basically, they can be divided into two important groups: discontinuous methods and continuous methods. Discontinuous methods rely on periodic measurements of chemical changes in the composition as a result of periodic exposure to UV-Vis light. These include infrared spectroscopy (FT-IR), [5] photoacoustic spectroscopy and Dynamic Mechanical Analysis (DMA) sensitometry [6–8]. These methods are mainly used to determine the degree of polymerisation and determine the number of unreacted monomers [9,10]. However, there are several disadvantages to these methods, such as time consuming and

low accuracy, due to the need to take representative samples of the material desired to study kinetics. Continuous methods rely on monitoring the progress of the photopolymerisation process in on-line time, i. e., in real-time. The Real-Time-FT-IR technique is particularly useful [11–13]. During the process, the disappearance of absorbance bands is monitored at a given wavenumber corresponding to the bands of a given functional group. This method, since it has a short response time, can be used to determine the conversion rates of polymerisation systems very quickly.

Thus, there are many ways to study kinetics and photopolymerisation progress, and such studies are extremely important in terms of the properties of the final product [14,15]. The goal is to obtain products of high quality and possible low price. It is worth noting that the photopolymerisation process is becoming more and more popular and finds several applications in various areas of life [16–21]. Initially, it was mainly used in the coating industry to obtain solvent-free adhesives, paints, and varnishes for the automotive and furniture industries [22–24]. Currently, photopolymerisation is used, among others in the

\* Corresponding author at: Department of Biotechnology and Physical Chemistry, Faculty of Chemical Engineering and Technology, Cracow University of Technology, Warszawska 24, 30-155 Kraków, Poland.

E-mail address: [jortyl@pk.edu.pl](mailto:jortyl@pk.edu.pl) (J. Ortyl).

<https://doi.org/10.1016/j.eurpolymj.2021.110612>

Received 22 May 2021; Received in revised form 21 June 2021; Accepted 22 June 2021

Available online 25 June 2021

0014-3057/© 2021 The Author(s).

Published by Elsevier Ltd.

This is an open access article under the CC BY-NC-ND license

(<http://creativecommons.org/licenses/by-nc-nd/4.0/>).

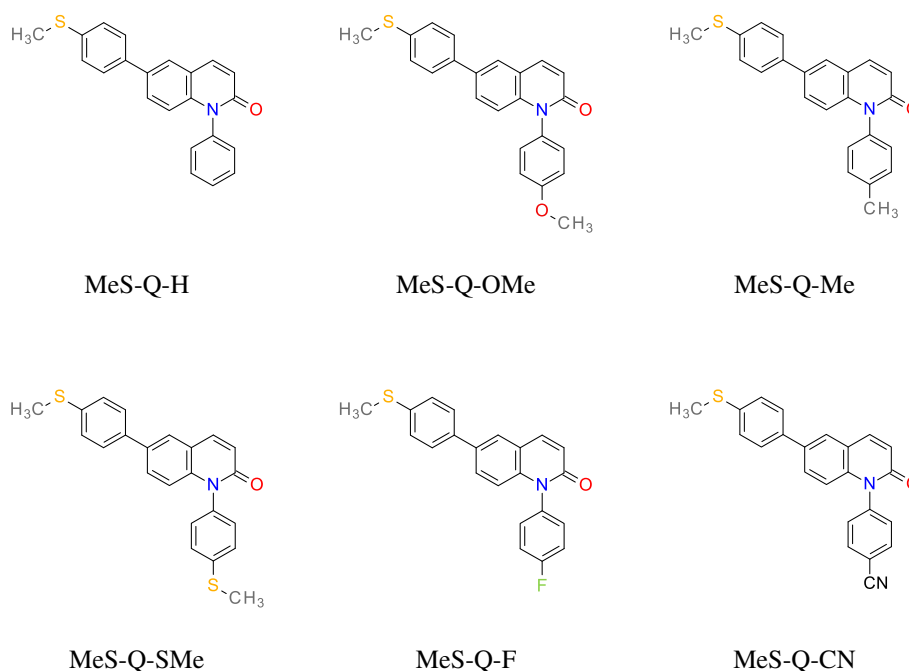


Fig. 1. Structures of molecular fluorescent sensors and photosensitizers for photopolymerisation processes.

printing industry for creating prints on plastic materials and other metals, [25] in microelectronic [26–29] for encapsulation of various integrated circuits, in dentistry, [30–33] in 3D printing technologies for designing and forming three-dimensional models [34–38]. Photopolymerisation is also increasingly used in medicine for the production of polymer hydrogels [33,39–43]. Photolithography is used to produce printed circuits, using photopolymerisation processes [44–46]. Such multiple applications of photopolymerisation processes contribute to the need to constantly search for more effective and more efficient substrates and initiating systems for photopolymerisation [15,47–53].

Therefore, in this work, new compounds, 6-(4-methylsulfanylphenyl)-1-phenylquinolin-2-one derivatives as a spectroscopic fluorescent probe for real-time monitoring of photopolymerisation and as photosensitizers for visible-curable fluorescent photopolymer resin for 3D printing are reported.

On the one hand, the quinolin-2-one derivatives were mainly suitable as sensors for monitoring the kinetics of various types of photopolymerisation processes [54]. On the other hand, they were slightly useful as sensitizers in two-component systems: the quinolin-2-one derivative/iodonium salt. Therefore, it was decided to modify the structure of quinolin-2-one, where at position 6, the electron-donor substituent 6-(4-methylsulfanylphenyl) was built into the basic chromophore - quinolin-2-one. The influence of this grouping on the effectiveness of both initiation in two-component systems and the usefulness of these compounds for the role of molecular fluorescent probes was investigated. Basic spectroscopic studies including absorbance, fluorescence emission and excitation spectra were carried out. Subsequently, a number of studies on the suitability of new compounds for the role of fluorescent molecular probes using Fluorescence Probe Technology (in short FPT) were performed [55–58]. Moreover, the article presents the research on the suitability of these compounds as co-initiators in a two-component system: derivative 6-(4-methylsulfanylphenyl)-1-phenylquinolin-2-one/4,4'-dimethyl-diphenyl iodonium hexafluorophosphate (OMNICAT 440). Cationic photopolymerisation processes of CADE epoxy and vinyl TEGDVE monomers, free-radical photopolymerisation of TMPTA acrylic monomer as well as thiol-ene photopolymerisation of mixture of monomers: TATATO / MERCAPTO when exposed to UV light with maximum emission at 365 nm and visible light with maximum emission at 405 nm were carried out.

## 2. Experimental

### 2.1. Materials

All chemicals and solvents employed in this investigation were at least of reagent grade and were used as received. Six derivatives of 6-(4-methylsulfanylphenyl)-1-phenylquinolin-2-one were synthesized and applied for the role of sensors and photosensitizers in a two-component initiating system based on 4,4'-dimethyl-diphenyl iodonium hexafluorophosphate (OMNICAT440). The following derivatives were applied for the studies 1-phenyl-6-(4-methylsulfanylphenyl)quinolin-2-one (MeS-Q-H), 1-(4-methoxyphenyl)-6-(4-methylsulfanylphenyl)quinolin-2-one (MeS-Q-OMe), 1-(4-methylphenyl)-6-(4-methylsulfanylphenyl)quinolin-2-one (MeS-Q-Me), 1,6-bis(4-methylsulfanylphenyl)quinolin-2-one (MeS-Q-SMe), 1-(4-fluorophenyl)-6-(4-methylsulfanylphenyl)quinolin-2-one (MeS-Q-F), 1-(4-cyanophenyl)-6-(4-methylsulfanylphenyl)quinolin-2-one (MeS-Q-CN). The studied details of synthesis and physicochemical data of the derivatives of 6-(4-methylsulfanylphenyl)-1-phenylquinolin-2-one are given in the Supporting Information. <sup>1</sup>H NMR and <sup>13</sup>C NMR spectra are presented in Figure S1-S12. The structures of these derivatives are shown in Fig. 1.

Molecular fluorescence sensors were used as a reference to monitor the progress of FPT photopolymerisation processes, 7-diethylamino-4-methylcoumarin (Coumarin 1, Sigma Aldrich) to monitor free radical and thiol-ene photopolymerisation processes, respectively.

For the cationic photopolymerisation triethylene glycol divinyl ether (TEGDVE, Sigma Aldrich) and 3,4-(epoxycyclohexane) methyl 3,4-epoxycyclohexylcarboxylate (CADE, Lambson), 4,4'-dimethyl-diphenyl iodonium hexafluorophosphate (OMNICAT 440, Alfa Aesar) were used as a model vinyl ether monomer, epoxide monomer and a photoinitiator, respectively. For the free-radical photopolymerisation trimethylolpropane triacrylate (TMPTA, Sigma Aldrich) and 2,2-dimethoxy-2-phenylacetophenone (DMPA, Sigma Aldrich) or 4,4'-dimethyl-diphenyl iodonium hexafluorophosphate (OMNICAT 440, Alfa Aesar), were employed as a methacrylate monomer and a free-radical photoinitiators. Furthermore, trimethylolpropane triacrylate (TMPTA, Sigma Aldrich) or 1,3,5-triallyl-1,3,5-triazine-2,4,6-trione (TATATO, Sigma Aldrich) and trimethylolpropane tris(3-mercaptopropionate) (MERCAPTO, Sigma

Aldrich) were utilized as monomers for the compositions polymerized by the thiol-ene mechanism. 2,2-dimethoxy-2-phenylacetophenone (DMPA, Sigma Aldrich) was used as the photoinitiator in the thiol-ene polymerisation process for Fluorescence Probe Technology experiments and 4,4'-dimethyl-diphenyl iodonium hexafluorophosphate (OMNICAT 440, Alfa Aesar) was used for FT-IR experiments. Structures of all compounds are presented in [Figure S13](#).

## 2.2. Spectral measurements

Absorption and fluorescence spectra of the 6-(4-methylsulfanylphenyl)-1-phenyl-quinolin-2-one were recorded in acetonitrile (Sigma Aldrich), using the SilverNova spectrometer (StellarNet, Inc., Tampa, FL, USA) in combination with a broadband tungsten-deuterium UV-Vis light source (StellarNet, Inc., Tampa, FL, USA), and a quartz cuvette with 1.0 cm optical path. Next, the absorbance data were converted into extinction coefficients, expressed in classical units [ $\text{dm}^3 \text{mol}^{-1} \text{cm}^{-1}$ ]. Fluorescence measurements were carried out using the same miniature spectrometer. The spectral characteristics of the sensors were measured in acetonitrile at 25 °C using 10 mm thick quartz cells. As a source of excitation, the UV-LED 320 nm (UVTOP315-BL-TO39, Roithner Laser Technik GmbH, Wien, Austria) light was used. The fibre optic cable, used for transmission of light from the measurement site to the spectrometer was made of PMMA optical fibre with 2 mm core (Fibrochem, Poland). Fluorescence emission and excitation spectra in different solvents (polarity experiments) were recorded using Quanta Master™ 40 spectrofluorometer (Photon Technology International (PTI), currently a part of Horiba) at varied excitation and observation wavelengths in the range of 200–800 nm.

## 2.3. Steady state Photolysis

During the steady state photolysis, cuvettes with the 6-(4-methylsulfanylphenyl)-1-phenyl-quinolin-2-one derivatives in acetonitrile were irradiated by the UV-LED-365 M365L2 (Thorlabs Inc., Tampa, FL, USA) emitting light with the wavelength at  $\lambda_{\text{max}} = 365 \text{ nm}$  (~14 mW/cm<sup>2</sup>) for 60 min. The source of light was powered by a DC2200 regulated power supply (Thorlabs Inc., Tampa, FL, USA). The UV-Vis spectra was recorded with the UV/Vis deuterium-halogen light source SL5 (StellarNet, Inc., Tampa, FL, USA). The photolysis of 6-diphenylquinolin-2-one derivatives in the presence of OMNICAT 440 ( $1.6 \cdot 10^{-1} \text{ mol dm}^{-3}$ ) were determined with the same parameters over 20 min.

## 2.4. Fluorescence quenching

Fluorescence quenching studies of 6-(4-methylsulfanylphenyl)-1-phenyl-quinolin-2-one derivatives that act as sensitizers were carried out using the Quanta Master™ 40 (Photon Technology International (PTI), currently a part of Horiba) at excitation located in the maximum absorption for these compounds. Different amounts of OMNICAT440 quenching agent were added to the 6-diphenylquinolin-2-one derivatives in acetonitrile. The solutions were diluted, and the concentration of quenching agent varied from 0 to  $3.0 \cdot 10^{-2} \text{ mol dm}^{-3}$ .

## 2.5. Electrochemical characteristic determination of oxidation and reduction potential

The oxidation potentials of the investigated 2,6-diphenylquinolin-2-one derivatives ( $E_{\text{ox}}$  vs Ag/AgCl) were carried out in acetonitrile by cyclic voltammetry with tetrabutylammonium hexafluorophosphate (0.1 M) (Sigma Aldrich) as a supporting electrolyte (Electrochemical Analyzer M161 and the Electrode Stand M164, MTM-ANKO, Cracow, Poland). The working electrode was a platinum disk, and the reference was a silver chloride electrode – Ag/AgCl; a scan rate of 0.1 V/s has been used; ferrocene was applied as a standard and the potentials were determined from half peak potentials. The Gibbs free energy change

$\Delta G_{\text{et}}$  for an electron transfer between the components of the bimolecular photoinitiating system was calculated using the classical Rehm–Weller equation (1)

$$\Delta G_{\text{et}} = F[E_{\text{ox}}(D/D^{v+}) - E_{\text{red}}(A^{\cdot-}/A)] - E_{00} - (Ze^2/\epsilon a) \quad (1)$$

where: F is the Faraday constant ( $F = 96485.33289(59) \text{ Cmol}^{-1}$ ),  $E_{\text{ox}}(D/D^{v+})$  is oxidation potential of the electron donor,  $E_{\text{red}}(A^{\cdot-}/A)$  the reduction potential of the electron acceptor,  $E_{00}$  – the excited state energy,  $(Ze^2/\epsilon a)$  the electrostatic interaction energy for the initially formed ion pair.

Parameter  $(Ze^2/\epsilon a)$  is generally considered negligible in polar solvents. The excited state energy was determined from the excitation and emission spectra using Quanta Master™ 40 spectrofluorometer (Photon Technology International (PTI), (currently a part of Horiba) at varied excitation wavelengths in the range of 200–800 nm.

## 2.6. Molecular orbital calculations

For calculating the energy gap between the first triplet energy ( $T_1$ ) and ground state energy ( $S_0$ ) Gaussian 09 package was used. First, the optimization of  $S_0$  and  $T_1$  states was carried out for each of the molecular structures of interest. Optimization of molecules in the ground state and first triplet excited state were performed using the density functional theory (DFT) method at a B3LYP/6-31G (d, p) level of theory. Energy gap was calculated as the difference of the total energy of the molecule in the first triplet excited state ( $E_{T1}$ ) and the total energy of the molecule in the ground state ( $E_{S0}$ ). The frontier molecular orbitals properties were analysed and visualized using GaussView 5.0 software.

## 2.7. Preparation of samples for monitoring the photopolymerisation processes by FPT

Samples for the study of photopolymerisation using the FPT method were prepared in vials of dark amber glass in a dark room by dissolution of the photoinitiator – OMNICAT440 and each fluorescent sensor – 6-(4-methylsulfanylphenyl)-1-phenyl-quinolin-2-one in the monomer in such proportions as to obtain the concentration 1.0% by weight of the photoinitiator and  $4.73 \cdot 10^{-3} \text{ mol/dm}^3$  of the sensor for radical photopolymerisation and  $4.91 \cdot 10^{-3} \text{ mol/dm}^3$  for thiol-ene photopolymerisation. Before measurement, two drops of the composition were placed in the middle of a microscope slide (75 mm × 25 mm × 1 mm, from Thermo Scientific), equipped with two 0.09 mm thick spacers located on the slide sides, and the slide was covered with another microscope slide to form a sandwich structure. Thickness of the samples was measured with an electronic micrometre. The slides were kept together using paper clips placed on their sides.

## 2.8. Monitoring the fluorescence changes during photopolymerisation

Apparatus to the Fluorescence Probe Technology was composed of a sample compartment, equipped with a specially designed sensor head where the sample was put, a Peltier cell-based thermostatic head, a miniature CCD spectrometer (SilverNova from StellarNet, Inc., Tampa, FL, USA), interfaced to a microcomputer for data acquisition, and a UV LED emitting at the wavelength  $\lambda_{\text{max}} = 320 \text{ nm}$  (UVTOP315-BL-TO39, Roithner Laser Technik GmbH, Austria) incorporated into the sensor head. The UV light from the LED illuminated about 5 mm spot within the thin-layer sample. The light from the measurement site was transferred to the spectrometer using a PMMA fibre optic cable with 2 mm core. The UV LED was supplied with constant current of 23 mA from the stabilized constant current source. Structure of the sample compartment with the sensor head and the appearance of the thermostatic head were similar to those reported previously; however, it has been modernized with the thermostat system that guarantees the stability of environmental conditions during the monitoring of the photopolymerisation process [59]. Therefore, all photopolymerisation processes were carried out at an

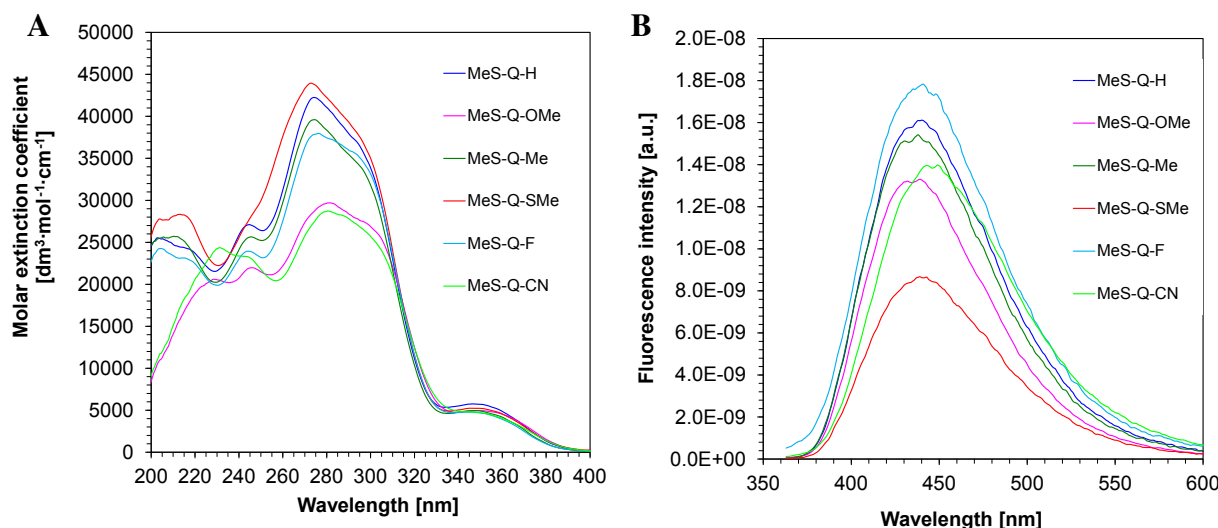


**Fig. 2.** Spectroscopic properties of 6-(4-methylsulfanylphenyl)-1-phenyl-quinolin-2-one derivatives: (A) UV-visible absorption spectra of the 6-(4-methylsulfanylphenyl)-1-phenyl-quinolin-2-one derivatives in acetonitrile; (B) fluorescence spectra of the 6-(4-methylsulfanylphenyl)-1-phenyl-quinolin-2-one derivatives in acetonitrile.

ambient temperature 25 °C using ITC4020 thermostat (Thorlabs Inc., Newton, NJ, USA). A photograph of the measurement system is shown in ref [60].

### 2.9. Preparation of samples for monitoring the photopolymerisation processes by FT-IR

Thin-layered compositions for the study of photopolymerisation using the real-time FT-IR method were prepared as well as the samples for the study of photopolymerisation using the FPT method. Each composition included the appropriate monomer (CADE, TEGDVE, TMPTA, mixture TATATO/MERACPTO 1:1 w/w%), the novel derivative of 6-(4-methylsulfanylphenyl)-1-phenyl-quinolin-2-one with a concentration of about  $4.8 \cdot 10^{-3} \text{ mol dm}^{-3}$  which constituted approx. 0.1% of the weight in relation to the total composition and iodonium salt with the concentration of 1.0% weight in the monomer.

### 2.10. Monitoring the photopolymerisation processes by Real-Time FT-IR

The kinetic of cationic photopolymerisation was investigated using the real-time FT-IR method along with FT-IR i10 NICOLET™ spectrometer with a horizontal adapter (Thermo Scientific, Waltham, MA, USA).

The measurement using the real-time-FT-IR technique consists in the fact that a drop of the composition based on the TEGDVE monomer, TMPTA, mixture of TATATO/MERACPTO was placed with a glass pipette between two polypropylene films, thus obtaining laminates. The films were pressed that to always achieve the same reproducible polymer coating thickness of  $25 \mu\text{m} \pm 10\%$ . Real-time-FT-IR measurements for compositions based on CADE monomer were made on a round BaF<sub>2</sub> pellet with a diameter  $25 = 25 \pm 0.2 \text{ mm} \times 5 \pm 0.1 \text{ mm}$ . The compositions were spread over the surface of the pellet with a glass pipette that the thickness was always also  $25 \mu\text{m} \pm 10\%$ . The compositions prepared on the BaF<sub>2</sub> pellet or laminates made of PP film, were placed in the holder made of metal, and then in the horizontal attachment mounted on the spectrometer. Photopolymerisation measurements were made using, the time of photopolymerisation was maximum 800 s. Measurements were carried out in a dark room where only lighting was used as the light source, which emits red radiation with  $\lambda_{\text{max}} = 650 \text{ nm}$ .

The light source for the real-time FT-IR method was the 365 nm M365L2, M365LP1 diodes and 405 nm M405L4 diode (Thorlabs Inc. U. S.), powered by DC2200 regulated power supply (from Thorlabs Inc. U.

S.). The UV-LED was started 10 s after the start of spectral registration. The distance between irradiation sources and formulations is 2,1 cm.

Because the decrease of absorption of the peak area is directly proportional to the number of polymerized groups, the degree of conversion of the function group was calculated by measuring the peak area at each time of the reaction by using Equation (2):

$$C_{FT-IR} [\%] = \left( 1 - \frac{A_{After}}{A_{Before}} \right) \cdot 100 \% \quad (2)$$

where:

$A_{Before}$  is an area of the absorbance peak characteristic for used monomer and type of photopolymerisation before polymerization process and;

$A_{After}$  is an area of the same absorbance peak, but after polymerisation process.

The values of the characteristic absorbance peak for studied monomers were given below for each type of photopolymerisation. The evaluation of vinyl group content was continuously followed in laminated conditions at about  $1634 \text{ cm}^{-1}$  (TEGDVE and TMPTA monomer). Moreover, the evolution of the epoxy group content was continuously followed under air at about  $790 \text{ cm}^{-1}$  (CADE monomer). The compositions which contain 1,3,5-triallyl-1,3,5-triazine-2,4,6-trione (TATATO) and MERCAPTO monomers (50%/50% w/w) were deposited on a BaF<sub>2</sub> pellet under air. The evolution of the thiol (S-H) group content was continuously monitored at approximately  $2570 \text{ cm}^{-1}$ . FT-IR also followed the double bond conversion of TATATO at about  $3083 \text{ cm}^{-1}$ . The molar ratio of thiol vs. allyl used in all experiments was 1: 1.6.

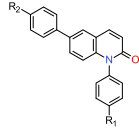
### 2.11. 3D printing experiment

For laser write and 3D printing experiments, a laser diode at 405 nm with an intensity of  $100 \text{ mW} \cdot \text{cm}^{-2}$  (spot size  $\sim 50 \mu\text{m}$ ) was used for the spatially controlled irradiation (NEJE DK-8-KZ 1000 mW Laser Engraver Printer). The photosensitive formulations (2 mm thickness) were deposited onto a microscope slide and was polymerised under air. Generated patterns were analysed by a numerical optical microscope (DSX-HRSU from OLYMPUS corporation).

### 2.12. Characterization of the 3D patterns by fluorescent microscopy

The generated 3D objects were observed thanks to an optical stereo

**Table 1**  
Spectral characteristics of the 6-(4-methylsulfanylphenyl)-1-phenyl-quinolin-2-one derivatives studied.

Serie	Acronym	R <sub>1</sub>	R <sub>2</sub>	Absorption characteristics				Emission characteristics at 350 nm excitation		$\Delta\nu$ Stoke's shift [cm <sup>-1</sup> ]
				$\lambda_{\text{max-ab}}$ [nm]	$\epsilon_{\text{max}}$ [dm <sup>3</sup> ·mol <sup>-1</sup> ·cm <sup>-1</sup> ]	$\epsilon_{365}$ [dm <sup>3</sup> ·mol <sup>-1</sup> ·cm <sup>-1</sup> ]	$\epsilon_{405}$ [dm <sup>3</sup> ·mol <sup>-1</sup> ·cm <sup>-1</sup> ]	$\lambda_{\text{max-fluo}}$ [nm]	$I_{\text{max}}$ [rel.u.]	
	MeS-Q-H	-H	MeS-	274	42,255	4024	131	440	1.61•10 <sup>-8</sup>	8719
	MeS-Q-OMe	-OMe	MeS-	281	29,696	4025	51	440	1.85•10 <sup>-8</sup>	9019
	MeS-Q-Me	-Me	MeS-	274	39,608	3441	104	438	1.54•10 <sup>-8</sup>	8715
	MeS-Q-SMe	-MeS	MeS-	273	43,954	3848	156	439	8.67•10 <sup>-9</sup>	8668
	MeS-Q-F	-F	MeS-	276	37,967	3248	128	441	1.78•10 <sup>-8</sup>	8477
	MeS-Q-CN	-CN	MeS-	280	28,730	3515	100	443	2.13•10 <sup>-8</sup>	9072

$\lambda_{\text{max-ab}}$  – position of absorption maximum for the long-wavelength band [nm].

$\epsilon_{\text{max}}$  – molar extinction coefficient measured at  $\lambda_{\text{max-ab}}$  [dm<sup>3</sup>·mol<sup>-1</sup>·cm<sup>-1</sup>].

$\epsilon_{365}$  – molar extinction coefficient measured at 365 nm [dm<sup>3</sup>·mol<sup>-1</sup>·cm<sup>-1</sup>].

$\epsilon_{405}$  – molar extinction coefficient measured at 405 nm [dm<sup>3</sup>·mol<sup>-1</sup>·cm<sup>-1</sup>].

$\lambda_{\text{max-fluo}}$  – position of maximum fluorescence intensity [nm].

$I_{\text{max}}$  – intensity of the fluorescence at  $\lambda_{\text{max-fluo}}$ .

microscope (Bresser Advance ICD 10–160 × Zoom Stereo-Microscope, Bresser GmbH, Germany) and DSX1000 from OLYMPUS and on an inverted fluorescence microscope Olympus IX83 equipped with X-line lenses and a monochrome camera Photometrics Prime BSI.

### 3. Results and discussion

#### 3.1. Spectroscopic properties of 6-(4-methylsulfanylphenyl)-1-phenyl-quinolin-2-one derivatives

Spectroscopic studies are extremely important to determine the effectiveness of new compounds for the role of both fluorescent probes and photosensitizers. One of the most important parameters in photopolymerisation processes is the compatibility of the absorption spectrum of photoinitiators with the emission spectrum of the light source. Commercially photoinitiators currently used in the industry require short-wavelength UV light (below 300 nm). For example, the maximum absorption of the 4,4'-dimethyl-diphenyl iodonium hexafluorophosphate (OMNICAT 440) in acetonitrile is at 240.6 nm (Figure S14). UV light sources adapted in industry emit energy above 350 nm, and they are not suitable for these processes because of mismatching between the absorption characteristic of the commercial photoinitiators and the emission characteristic of the light sources. In these cases, polymerisation is inefficient. Thus, the spectral properties of the photoinitiating system have a significant impact on polymerisation rate, which is connected with the amount of absorbed light. The quinolin-2-one absorb to the 400 nm range, so the spectrum of the absorption of the new compound overlaps with the emission spectra of the maximum of medium-pressure mercury lamps, and with the emission of UV-A-LED with a maximum at 365 nm (Fig. 2A). On the other hand, all 6-(4-methylsulfanylphenyl)-1-phenyl-quinolin-2-one derivatives had a sufficient fluorescence intensity (Fig. 2B, Table 1) for their spectral characteristics, which was easily measured at a probe concentration of ca. 0.1% by weight and a sample thickness of ca. 0.1 mm. Fluorescence sensors should present the strongest fluorescence possible (i.e., not less than 1000 [absolute units] for this spectrometer) when excited with a light wavelength of 320 nm when they are to be used in FPT technology. The wavelength selection is not accidental, as when the excitation light with shorter wavelengths is used, their intensity is strongly attenuated by the microscope glass slides that are normally used for preparing thin-layered samples in FPT.

Moreover, the results of computer simulations confirm the assumptions about the nature of the occupation of molecular orbitals in the analysed molecules. HOMO orbitals predominate in essentially entire molecules except for the substituted N-phenyl ring. Even the addition of

other nucleophilic groups on the opposite side of the molecule, such as a methoxy group (MeS-Q-OMe), does not significantly affect the displacement of HOMO orbitals in the molecule due to the weaker nucleophilic nature of these groups compared to the thiomethyl group. Orbital visualizations were presented in the supplement.

In addition, molecular sensors, in order to be used for kinetic studies of photopolymerisation processes as molecular sensors, should, in particular, respond to changes in polarity. As a result of the photopolymerisation process, a decrease in the polarity of the system is usually observed, because the double bonds in the monomer are transformed into single bonds that are less polar. Molecular probes as electron-donor-electron-acceptor systems on a coupled bond system (for example an aromatic system) have a low dipole moment in the ground state, while in the excited state they show a very high dipole moment due to intramolecular electron transfer. In addition, the more polar a given system is, the lower the energy due to rotation in the polar medium is observed, with the decrease in energy along with the increase in excited state polarity being greater than the decrease in ground energy. Therefore, the energy difference between the excited and ground states decreases, the polarity of the system increases, and this results in a shift in fluorescence emission towards longer waves. In the case of polymerisation, the opposite is observed, a decrease in the polarity of the system is observed and the molecular probes shift their fluorescence spectrum, generally in the direction of shorter waves.

In order to check whether the compounds are sensitive to changes in polarity, studies on solvatochromic effects are performed. This phenomenon illustrates the effect of solvents on the electronic spectra of fluorescent compounds. The solvatochromic effect is associated with a change in the energy of the particle in solution compared to the energy of the free molecule. The energy of this molecule consists of a dispersion interaction, mainly particle polarization, electrostatic interaction, as well as the solvent Stark effect. The Stark effect occurs when a solvent fluctuation occurs in an approximately dissolved non-polar particle, which leads to the formation of a temporary, weak electric field [61].

The influence of solvent polarity changes on the characteristics of emission spectra and excitation of selected potential molecular probes based on quinolin-2-one derivatives was tested using the  $E_N^T$  scale. Scale  $E_N^T$  is based on the assumption that the least polar solvent is tetramethylsilane (TMS) and has a value of 0, while water is the most polar solvent and has a value of 1. The value of  $E_N^T$  is calculated from the following Equation (3): [62]

$$E_N^T = \frac{E_T(\text{solvent}) - E_T(\text{TMS})}{E_T(\text{water}) - E_T(\text{TMS})} = \frac{E_T(\text{solvent}) - 30,7}{32,4} \quad (3)$$

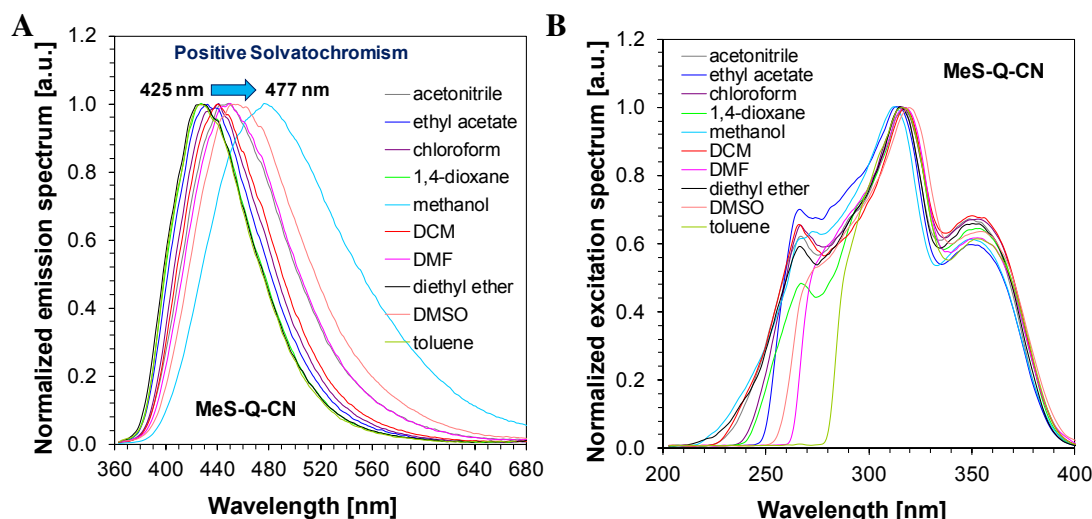


**Fig. 3.** (A) Normalized emission spectrum for 1-(4-cyanophenyl)-6-(4-methylsulfanylphenyl)quinolin-2-one MeS-Q-CN in solvents of different polarity; (B) Normalized excitation spectrum for 1-(4-cyanophenyl)-6-(4-methylsulfanylphenyl)quinolin-2-one MeS-Q-CN in solvents of different polarity. In addition, a correlation was also performed between the solvent polarity using the  $E_N^T$  scale and the intensity of the emission spectrum and excitation spectrum, and a linear relationship was obtained (Fig. 4, Table 2).

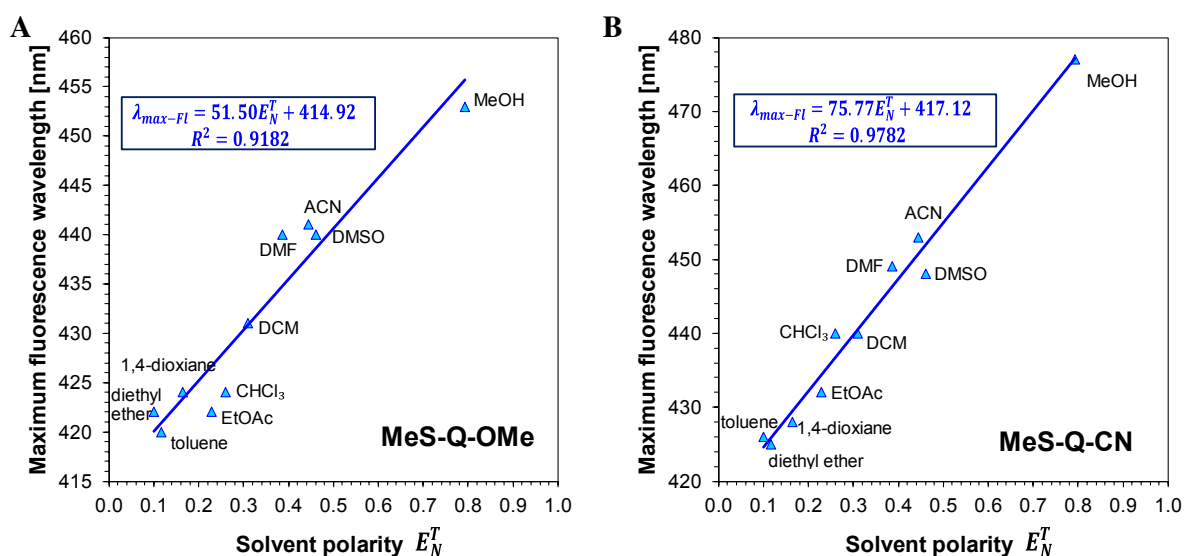


**Fig. 4.** Dependence of the location of the maximum intensity of the emission spectrum for (A) the 1-(4-methoxyphenyl)-6-(4-methylsulfanylphenyl)quinolin-2-one (MeS-Q-OMe) on the polarity of the solvents (scale  $E_N^T$ ); (B) the 1-(4-cyanophenyl)-6-(4-methylsulfanylphenyl)quinolin-2-one (MeS-Q-CN) derivative on the polarity of the solvents (scale  $E_N^T$ ).

As the solvent polarity increases, the bathochromic shift of the emission spectra of 1-(4-methoxyphenyl)-6-(4-methylsulfanylphenyl)quinolin-2-one (MeS-Q-OMe) and 1-(4-cyanophenyl)-6-(4-methylsulfanylphenyl)quinolin-2-one (MeS-Q-CN) in the direction of longer waves was observed (Fig. 3A and S21). On the other hand, in the case of excitation spectra in different solvents, no significant changes in their characteristics were observed (Fig. 3B and S22).

### 3.2. Applicability of 6-(4-methylsulfanylphenyl)-1-phenyl-quinolin-2-one derivatives for on-line progress monitoring of free-radical and thiol-ene photopolymerisation processes

Due to the fact that selected 6-(4-methylsulfanylphenyl)-1-phenyl-quinolin-2-one derivatives are sensitive to changes in polarity, the compounds for the role of fluorescent sensors using Fluorescent Probe Technology (FPT) was studied. The progress of the photopolymerisation

process using the FPT technique was monitored using parameter R. Parameter R illustrates the change in shift of emission spectra during irradiation. Parameter R is defined as the ratio of fluorophore fluorescence intensity measured at two different wavelengths, which are located on both sides of the maximum fluorescence spectrum derived from the analysed compound. In this case, the ratio R was determined by dividing the intensity at the shorter wavelength  $I_1$  by the intensity at the longer wavelength  $I_2$ . It is a parameter used to constantly monitor the progress of very fast processes such as photopolymerisation [55]. The basic advantage of using the parameter R is the ability to measure the ratio intensity accurately. This can be ascribed to the fact that when the lengths of the waves arranged on both sides of the fluorescence spectrum maximum are appropriately selected, the fluorescence intensity ratio is a linear function of the degree of conversion of monomer function groups [61–64]. The method of determining the R parameter is illustrated in Fig. 5.

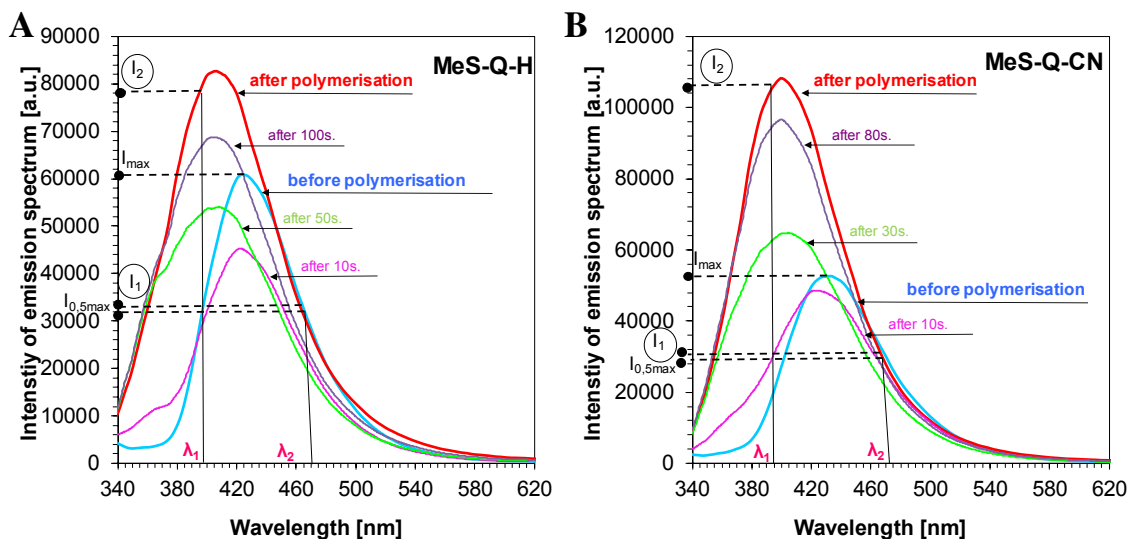


**Fig. 5.** Changes of fluorescence spectra of (A) MeS-Q-H sensor during free-radical photopolymerisation of TMPTA monomer under irradiation 320 nm, ( $\lambda_1$ ,  $\lambda_2$  are monitoring wavelengths); (B) MeS-Q-CN sensor during free-radical photopolymerisation of TMPTA monomer under irradiation 320 nm, ( $\lambda_1$ ,  $\lambda_2$  are monitoring wavelengths).

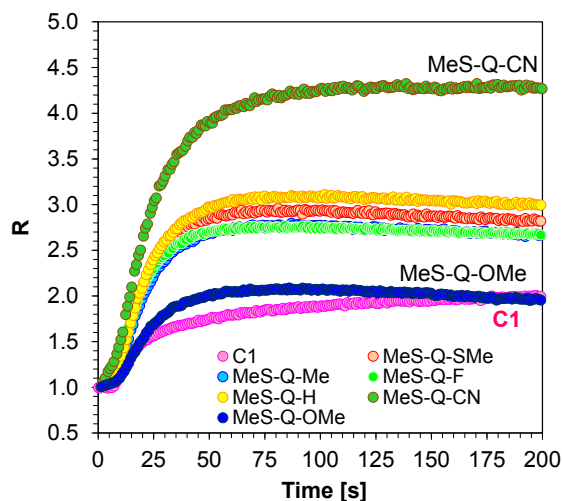


**Fig. 6.** Monitoring free-radical photopolymerisation of TMPTA monomer under 320 nm by FPT, using the 6-(4-methylsulfanylphenyl)-1-phenyl-quinolin-2-one derivatives as the fluorescent sensors and Coumarin 1 (C1) as a reference probe.

The radical photopolymerisation process of the model TMPTA monomer was carried out for 200 s when exposed to UV-LED with a maximum emission of 320 nm. During the radical photopolymerisation process, a shift in the emission spectrum from 6-(4-methylsulfanylphenyl)-1-phenyl-quinolin-2-one derivatives towards shorter wavelengths was observed. In addition, the coating was completely cured after about 75 s, because after this time a plateau of kinetic profiles was obtained (Fig. 6). The sensitivity of the tested probes was also compared with the well-known commercial coumarin 1. The relative sensitivity of the tested probes was calculated from the following Equation (4):

$$S_{rel} = \frac{\left[ \frac{(R_{max} - R_0)}{R_0} \right]}{\left[ \frac{(R_{max-ref} - R_{0-ref})}{R_{0-ref}} \right]} \quad (4)$$

$R_0$  – R value for the analysed sensor in the composition before photopolymerisation

$R_{max}$  – R value for the analysed sensor in the composition after photopolymerisation

$R_{0-ref}$  – R value for the reference sensor in the composition before photopolymerisation

$R_{max-ref}$  – R for the reference sensor in a photo-cured composition

The calculated sensitivity values are given in Table 3. All of the new

**Table 2**

Summarized data of excitation and emission spectra of solutions of compound MeS-Q-OMe and MeS-Q-CN.

Solvent	$E_N^T$	MeS-Q-CN		MeS-Q-OMe	
		Excitation spectrum $\lambda_{max-ex}$ [nm]	Emission spectrum $\lambda_{max-fl}$ [nm]	Excitation spectrum $\lambda_{max-ex}$ [nm]	Emission spectrum $\lambda_{max-fl}$ [nm]
acetonitrile	0.460	349	448	351	440
ethyl acetate	0.228	350	432	353	422
chloroform	0.259	353	440	353	424
1,4-dioxane	0.164	353	428	354	424
methanol	0.762	350	477	352	453
DCM (dichloromethane)	0.309	350	440	351	431
DMF (dimethylformamide)	0.386	352	449	353	440
diethyl ether	0.117	350	425	353	420
DMSO (dimethyl sulfoxide)	0.444	355	453	331	441
Toluene	0.099	352	426	352	422

$E_N^T$  – scale of polarity [8].

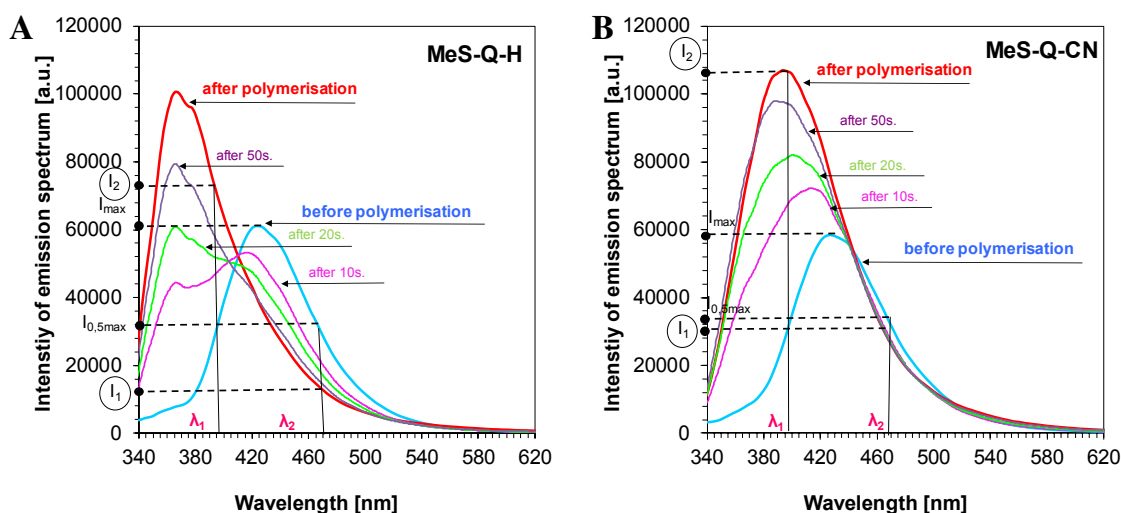
$\lambda_{max-ex}$  – wavelength for the maximum intensity of the excitation spectrum [nm].

$\lambda_{max-fl}$  – wavelengths for the maximum intensity of the emission spectrum [nm].

Table 3

Spectroscopic data of 6-(4-methylsulfonylphenyl)-1-phenyl-quinolin-2-one derivatives during the photopolymerisation processes.

Sensor	$\lambda_{\text{max-BEFORE}}$ [nm]	Intensity @ $\lambda_{\text{max-BEFORE}}$ [a.u.]	$\lambda_{\text{max-AFTER POL}}$ [nm]	Intensity @ $\lambda_{\text{max-AFTER}}$ [a.u.]	$ \Delta I_{\text{max}} $ [a.u.]	$\Delta I_{\text{max}}^a$ [%]	$\Delta \lambda_{\text{max}}$ [nm]	Relative sensitivity <sup>b</sup>
<b>Free-radical photopolymerisation process of TMPTA under 320 nm</b>								
MeS-Q-H	423.5	60,848	406.1	82,674	-21826	-36	-17.4	1.99
MeS-Q-OMe	424.4	56,446	416.8	45,125	11,321	20	-7.6	1.02
MeS-Q-Me	424.4	59,449	411.9	81,579	-22130	-37	-12.5	1.71
MeS-Q-SMe	425.8	49,963	411.9	73,044	-23081	-46	-13.8	1.87
MeS-Q-F	422.6	52,707	405.2	92,123	-39416	-75	-17.4	1.69
MeS-Q-CN	433.4	52,636	399.4	108,232	-55595	-106	-33.9	3.14
C1-ref.	425.8	617,546	419.5	397,064	220,482	36	-6.3	1.00
Sensor	$\lambda_{\text{max-BEFORE}}$ [nm]	Intensity @ $\lambda_{\text{max-BEFORE}}$ [a.u.]	$\lambda_{\text{max-AFTER}}$ [nm]	Intensity @ $\lambda_{\text{max-AFTER}}$ [a.u.]	$ \Delta I_{\text{max}} $ [a.u.]	$\Delta I_{\text{max}}^a$ [%]	$\Delta \lambda_{\text{max}}$ [nm]	Relative sensitivity <sup>b</sup>
<b>Thiol-ene photopolymerisation process of TMPTA/MERCAPTO (50/50 %w/w) under 320 nm</b>								
MeS-Q-H	423.5	61,085	398.6	65,753	-4668	-8	-25.0	3.03
MeS-Q-OMe	424.0	56,850	399.4	50,535	6315	11	-24.5	1.59
MeS-Q-Me	423.5	59,592	397.7	60,047	-456	-1	-25.9	2.28
MeS-Q-SMe	424.9	54,391	397.2	53,742	649	1	-27.7	1.78
MeS-Q-F	422.2	54,792	398.1	67,662	-12869	-23	-24.1	3.90
MeS-Q-CN	427.1	58,453	399.0	106,274	-47821	-82	-28.1	2.84
C1-ref.	430.7	611,736	421.3	562,707	49,029	8	-9.4	1.00

<sup>a</sup> Changes in fluorescence intensity expressed as a percentage in relation to the initial value before polymerisation.<sup>b</sup> Relative sensitivity  $S_{\text{rel}}$  as a reference sensor Coumarin 1 was used.Fig. 7. Changes of fluorescence spectra during thiol-ene photopolymerisation of TMPTA/MERCAPTO (05%/05% w/w) monomers under irradiation 320 nm, ( $\lambda_1$ ,  $\lambda_2$  are monitoring wavelengths) for: (A) MeS-Q-H; (B) Q-MeS-Q-CN.

analysed probes are more sensitive than the commercial compound coumarin 1. The MeS-Q-CN probe shows the highest sensitivity to environmental changes. Its relative sensitivity is 3.14. The lowest sensitivity is for the MeS-Q-OMe ( $S_{\text{rel}} = 1.02$ ), thus for a compound having a strongly electron-donor substituent. The incorporation of different substituents into the quinolin-2-one structure has an effect on the value of sensitivity.

Moreover, the fluorescence intensity of these sensors was increasing during the photopolymerisation of the TMPTA monomer. This is due to the fact that as the system viscosity increases, the quantum fluorescence efficiency increases. The increased quantum fluorescence efficiency is caused by the reduction of the competitive process of non-radiative excitation of energy of the excited state. Therefore, in a high-viscosity environment, the excited sensor does not have such a large freedom of dissipation of excitation energy between the vibration and rotation states of the molecule, as in the case of low-viscosity solutions, hence the increase in fluorescence intensity during the photopolymerisation process was observed (Table 2, Fig. 5 and S23-S27).

Analogous measurements using new potential probes, 6-(4-methylsulfonylphenyl)-1-phenyl-quinolin-2-one derivatives were used to carry out the photopolymerisation process of thiol-ene acrylate monomer (TMPTA) and thiol (MERCAPTO) monomers (0.5 / 0.5% by weight). The R parameter was used for on-line monitoring of thiol-ene photopolymerisation progress, just like in the case of free-radical photopolymerisation (Fig. 7).

Very similar relationships as in the case of radical photopolymerisation were observed. First, all of the analysed probes are more sensitive compared to commercially available coumarin 1. Secondly, the type of built-in substituent for the analysed probes has an impact on the relative sensitivity values. A lower sensitivity was noted for a compound having a strongly electron-donor substituent, nevertheless higher compared to the commercially available probe - Coumarin 1 (Fig. 8). The increase in fluorescence intensity during the photopolymerisation process for all probes was also noted (Fig. 7, and S28-S32).



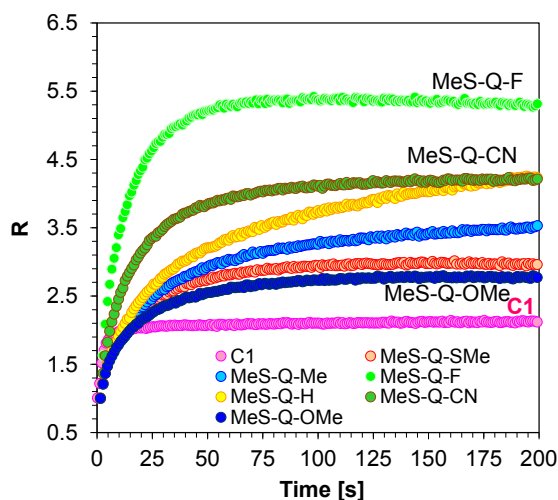


**Fig. 8.** Monitoring thiol-ene photopolymerisation of TMPTMA/MERCAPTO (0,5%/0,5% w/w) monomers under 320 nm by FPT, using molecular fluorescent sensors based on 6-(4-methylsulfanylphenyl)-1-phenyl-quinolin-2-one derivatives.

### 3.3. 6-(4-methylsulfanylphenyl)-1-phenyl-quinolin-2-one derivatives as a component of bimolecular and three molecular photoinitiating systems for photopolymerisation processes

Due to the fact that spectroscopic studies showed that 6-(4-methylsulfanylphenyl)-1-phenyl-quinolin-2-one derivatives absorb up to the visible range, they were tested as co-initiators in a two-component system quinolin-2-one derivative and iodonium salt, as accelerators of photopolymerisation processes of various types.

For this reason, measurements of monitoring of cationic photopolymerisation of vinyl monomer TEGDVE and epoxy monomer CADE were carried out at the wavelength in the UV-A range with a maximum emission of 365 nm and in the Vis range with a maximum emission of 405 nm. Additionally, measurements of radical photopolymerisation of triacrylate monomer and photopolymerisation of thiol-en of TATATO and MERCAPTO monomers were carried out at the wavelength in the UV-A range with a maximum emission of 365 nm and in the Vis range with a maximum emission of 405 nm. Widely available iodine salt in the form of 4,4'-dimethyl-diphenyl iodonium hexafluorophosphate (OMNICAT 440) has been used as a photoinitiator to monitor the polymerisation of various types. The absorption characteristics of the

photoinitiator are in the UV-C and UV-B range with a maximum at  $\lambda_{\max} = 242.29$  nm. Thus, the initiator's sensitivity is in the range of short wavelengths of UV light, which is a serious process problem, because photopolymerisation cannot occur at longer UV-A or visible light wavelengths when this type of compound is used. This problem can be solved by using appropriate photosensitizers, whose absorption characteristics are in the longer wavelength range than the iodonium photoinitiator. In this approach, the polymerisation of various types at a longer wavelength, in the range above 350 nm, which is not absorbed by the iodine salt, can be initiated by photosensitisation by electron transfer. With an appropriately selected photosensitizer, photoinduced electron transfer (PET) is possible. PET is an endothermic energy transfer process in which the absorbed quantum light initiates the transfer of electrons from the donor molecule - co-initiator to the acceptor molecule - iodine salt, OMNICAT 440 photoinitiator.

The real-time FT-IR method was used to monitor cationic photopolymerisation to identify final monomer conversions. Disappearance of vinyl monomer bands (TEGEVE) at a wave number of about  $1634\text{ cm}^{-1}$  was observed during the cationic photopolymerisation process. The number of waves corresponds to the disappearance of the double bonds in the monomer. The process was initiated using UV-LED as a light source that emitted electromagnetic radiation with a maximum wavelength  $\lambda_{\max} = 365$  nm and visible light with a maximum wavelength of 405 nm. Based on the recorded curves, it has been shown that all derivatives are suitable as co-initiators for the cationic photopolymerisation process of the vinyl monomer TEGDVE. The achieved conversion rates ranged from 75 – 90% both when irradiating the system with a diode with a maximum wavelength  $\lambda_{\max} = 365$  nm and 405 nm (Fig. 9). For individual co-initiators slight differences in the achieved conversion rates were observed. Nevertheless, the lowest conversion rates were noted for a compound having a strongly electron withdrawing substituent in the cyano form. Modification of the quinolin-2-one base ring (Article [54]) contributed to a significant increase in vinyl monomer conversion rates using much lower light output. Compounds with strong electron-donor-like groups, in the form of -MeS group in their structure and attached to a phenyl ring embedded in the 6-(4-methylsulfanylphenyl)-1-phenyl-quinolin-2-one chromophore at position 6 are better co-initiators (Fig. 10) compared to others findings found in the literature [54].

The developed photoinitiating systems are also suitable in the polymerisation reactions of the CADE epoxy monomer (Fig. 11 and S45-S50). The calculated conversions of the epoxy monomer are about 40%, when exposed to 365 nm UV diode. Final conversion values and the induction time are very similar for all compounds and their values are presented in Table 4.

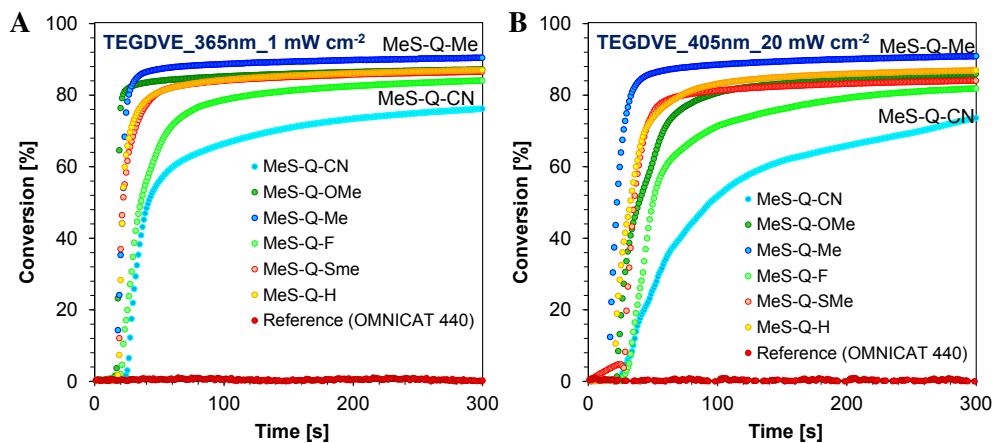


**Fig. 9.** Polymerization profiles of TEGDVE (vinyl function conversion vs. irradiation time) in the presence of different photoinitiating systems based on 4,4'-dimethyl-diphenyl iodonium hexafluorophosphate (OMNICAT 440, 1%) and 6-(4-methylsulfanylphenyl)-1-phenyl-quinolin-2-one derivatives (0.1%): (A) upon exposure to the LED@365 nm ( $1\text{ mW cm}^{-2}$ ) and (B) upon exposure to the LED@405 nm ( $20\text{ mW cm}^{-2}$ ) The irradiation starts at  $t = 10$  s.

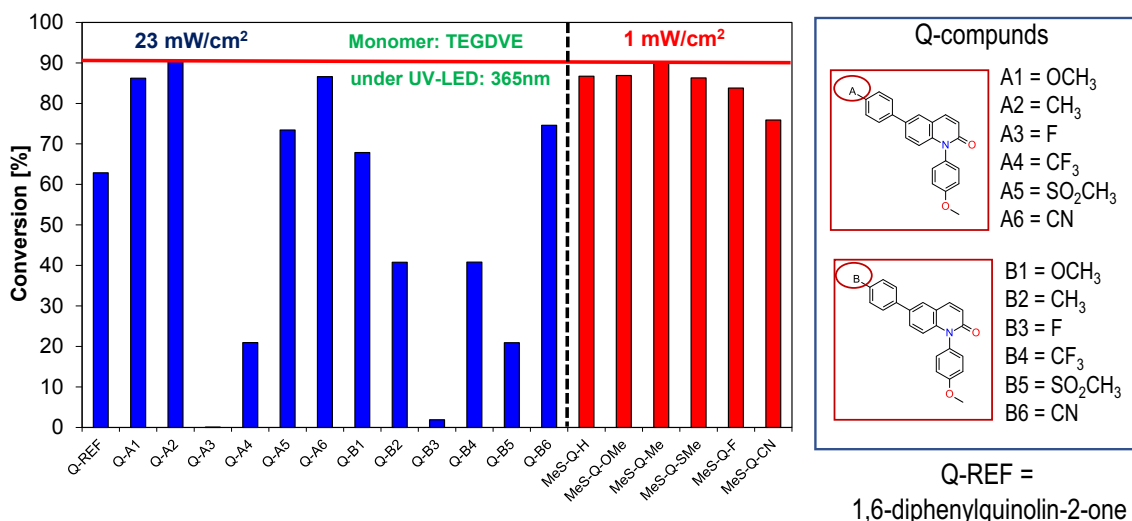


**Fig. 10.** Comparison of degrees of photopolymerisation conversion of the TEGDVE monomer upon exposure to the LED@ 365 nm using two-component initiating systems based on 4,4'-dimethyl-diphenyl iodonium hexafluorophosphate (OMNICAT 440, 1%) and 1,6-diphenylquinolin-2-one derivatives (0.1%), presented in article [54] (blue bar) with modified initiating systems presented in this article (red bars).

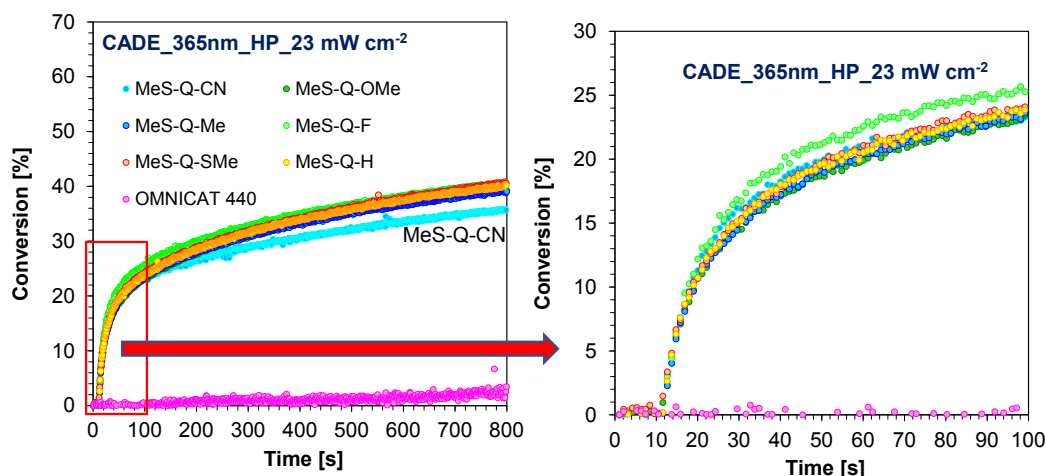


**Fig. 11.** Polymerisation profiles of CADE (epoxy function conversion vs. irradiation time) upon exposure to the LED@365 nm in the presence of different photo-initiating systems based on 4,4'-dimethyl-diphenyl iodonium hexafluorophosphate (OMNICAT 440, 1%) and 6-(4-methylsulfonylphenyl)-1-phenyl-quinolin-2-one derivatives (0.1%). The irradiation starts at  $t = 10$  s.

The developed photoinitiation systems also fulfil their role as polymerisation reactions of the TMPTA acrylate monomer (Fig. 12 and S51-S62). The calculated conversions of the double bonds of the acrylate monomer range from about 15% for MeS-Q-CN to 40% for MeS-Q-Me and MeS-Q-H upon exposure to the LED@365 nm with a maximum emission of 365 nm. Conversely, double bond acrylate monomer conversions range from about 30% for MeS-Q-CN to 60% for MeS-Q-OMe upon exposure to the LED@405 nm with a maximum emission of 405 nm. In each case, the lowest conversion rates were reported for the compound having a strongly electron withdrawing substituent, -CN.

Two-component initiating systems also show the ability to initiate photopolymerisation processes thiol-ene 1,3,5-triallyl-1,3,5-triazine-2,4,6-trione monomer (TATATO) and thiol monomer tris (3-mercaptopropionate) trimethylolpropane (MERCAPTO) when exposed to UV light with maximum emission at 365 nm and visible light with maximum emission at 405 nm (Figures S63-S74). Excellent conversion rates for the tested systems are shown in Fig. 13A (for UV radiation with a maximum emission of 365 nm) and Fig. 13B (for visible radiation with a maximum emission of 405 nm). In both cases, the conversion for thiol function is higher than for double allyl group bonds. The molar ratio of

functional groups was thiol: allyl 1: 1.6, respectively. Accordingly, the photopolymerisation of thiol-ene is not sensitive to oxygen, the photopolymerisation process was carried out only on barium fluoride pastilles. In addition, conversion rates for all analyzed two-component initiating systems: the 1,6 diphenylquinolin-2-one / iodonium salt in the form of OMNICAT 440 are comparable. This is due to the fact that the  $\Delta G_{et(S)}$  value for all systems is comparable. They are  $-1.24$  eV for MeS-Q-SMe to  $1.29$  eV for MeS-Q-OMe. In addition, the molar extinction coefficients at 365 nm and 405 nm for all analyzed new compounds have comparable values (Table 4).

#### 3.4. Photochemical mechanism of bimolecular photoinitiating systems consist of 6-(4-methylsulfonylphenyl)-1-phenyl-quinolin-2-one derivatives

The initiation of photopolymerisation by a two-component system consisting of quinolin-2-one derivatives and iodonium salt (OMNICAT 440) occurs through an electron transfer mechanism. Electron transfer from the quinolin-2-one derivative molecule to the corresponding iodonium salt (i.e., OMNICAT 440) is possible when the Gibbs free energy change ( $\Delta G_{et(S)}$ ) is negative.  $\Delta G_{et(S)}$  accompanies the electron transfer in the

**Table 4**

Functional group conversions of vinyl monomer for TEGDVE, epoxy monomer for CADE, acrylate monomer for TMPTA, and allyl monomer for TATATO and thiol monomer for MERCAPTO and using photoinitiating system based on 4,4'-dimethyl-diphenyl iodonium hexafluorophosphate (OMNICAT 440, 1%) and 6-(4-methylsulfanylphenyl)-1-phenyl-quinolin-2-one derivatives (wt. 0.1%) in the role of photosensitizers at 365 nm and/or 405 nm exposure.

Fluorescent sensor / Photosensitizer	$\epsilon$ @365 <sub>ab-365</sub> [dm <sup>3</sup> ·mol <sup>-1</sup> ·cm <sup>-1</sup> ]	$\epsilon$ @405 <sub>ab-405</sub> [dm <sup>3</sup> ·mol <sup>-1</sup> ·cm <sup>-1</sup> ]	Conversion [%]								
			CATIONIC PHOTOPOLYMERISATION				FREE-RADICAL PHOTOPOLYMERISATION				
			Epoxy monomer CADE	Vinyl monomer TEGDVE	Acrylate monomer TMPTA	TATAO/MERCAPTO @365 nm 0.1 [mW cm <sup>-2</sup> ]	TATAO/MERCAPTO @405 nm 2 [mW cm <sup>-2</sup> ]	Thiol Allyl	Thiol Allyl		
	@365 nm 23 mW cm <sup>-2</sup>	@365 nm 1 mW cm <sup>-2</sup>	@405 nm 20 mW cm <sup>-2</sup>	@365 nm 3.8 mW cm <sup>-2</sup>	@405 nm 20 mW cm <sup>-2</sup>						
MeS-Q-H	4024	131	40.4	86.7	88.1	40.4	52.3	~100	64.4	91.5	63.7
MeS-Q-OMe	4025	51	39.6	86.9	87.5	34.5	60.0	93.9	65.1	87.4	62.3
MeS-Q-Me	3441	104	39.4	90.2	92.1	39.8	42.2	~100	68.4	85.6	64.3
MeS-Q-SMe	3848	156	40.8	86.3	85.0	29.7	49.8	92.6	63.3	87.6	64.9
MeS-Q-F	3248	128	40.7	83.8	84.4	36.1	40.8	99.8	62.9	90.7	60.8
MeS-Q-CN	3515	100	35.9	75.9	82.0	15.1	35.8	99.2	64.7	87.1	59.6

$\epsilon$ @365<sub>ab-365</sub> – molar extinction coefficient measured at 365 nm [dm<sup>3</sup>·mol<sup>-1</sup>·cm<sup>-1</sup>].

$\epsilon$ @405<sub>ab-405</sub> – molar extinction coefficient measured at 405 nm [dm<sup>3</sup>·mol<sup>-1</sup>·cm<sup>-1</sup>].

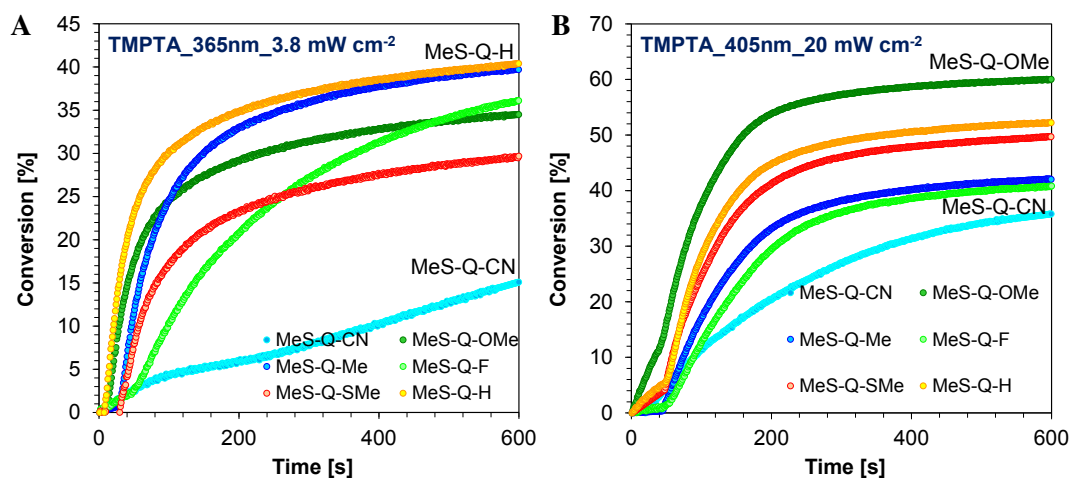


**Fig. 12.** Polymerisation profiles of TMPTA (acrylate function conversion vs. irradiation time) in the presence of different photoinitiating systems based on 4,4'-dimethyl-diphenyl iodonium hexafluorophosphate (OMNICAT 440, 1%) and 6-(4-methylsulfanylphenyl)-1-phenyl-quinolin-2-one derivatives (0.1%): (A) upon exposure to the LED@365 nm (3.8 mW cm<sup>-2</sup>); (B) upon exposure to the LED@405 nm (20 mW cm<sup>-2</sup>); The irradiation starts at t = 10 s.

initiation systems. The free energy ( $\Delta G_{\text{et(S)}}$ ) values for these initiating systems were calculated using the Rehm–Weller equation. The energy of singlet state ( $E_{00}$ ) was determined based on measurements of excitation and emission spectra (Fig. 14A and S15-S20).

The calculated  $\Delta G_{\text{et(S)}}$  values in each case are negative, which means that the process of electron transfer from the sensitizer to the iodonium salt is thermodynamically allowed. Therefore, these systems can be used to effectively initiate photopolymerisation processes.  $\Delta G_{\text{et(S)}}$  values ranged from 1.24 eV for MeS-Q-SMe to 1.29 eV for MeS-Q-OMe. The electron transfer process is most efficient for the MeS-Q-OMe compound. All thermodynamic and electrochemical data are included in Table 5. Cyclic voltammogram curves of compounds oxidation and reduction in acetonitrile were presented in Fig. 14B and S99-S100.

The next step was to perform fluorescence quenching measurements of the fluorophore (sensitizer) after adding the appropriate amount of quencher (OMNICAT 440 iodine salt) (Fig. 15 and S75 – S86). The Stern Volmer coefficient values were calculated based on a standard Equation (5):

$$\frac{I_0}{I} = 1 + K_{\text{SV}}[Q] \quad (5)$$

The calculated  $K_{\text{SV}}$  values for the tested initiating systems oscillated around 32 to 51 M<sup>-1</sup>. In addition, electron transfer quantum yields from the excited singlet state ( $\Phi_{\text{et(S)}}$ ) were also calculated based on Equation (6):

$$\Phi_{\text{et(S)}} = \frac{K_{\text{SV}}[Q]}{K_{\text{SV}}[Q] + 1} \quad (6)$$

The  $\Phi_{\text{et(S)}}$  values oscillated between 0.37 and 0.49 for all quinolin-2-one derivatives. These values suggest that quinolin-2-on can react not only act through a singlet state pathway but also from the triplet state.

In addition, these compounds are stable when exposed to 365 nm UV radiation (14mW / cm<sup>2</sup>) for up to 60 min (Fig. 16A and S87, S89, S91, S93, S95). Only after adding the OMNICAT 440 photoinitiator, the photosensitizer absorption spectrum changes when exposed to 365 nm UV radiation (14mW / cm<sup>2</sup>) within 20 min (Fig. 16B and S88, S90, S92,

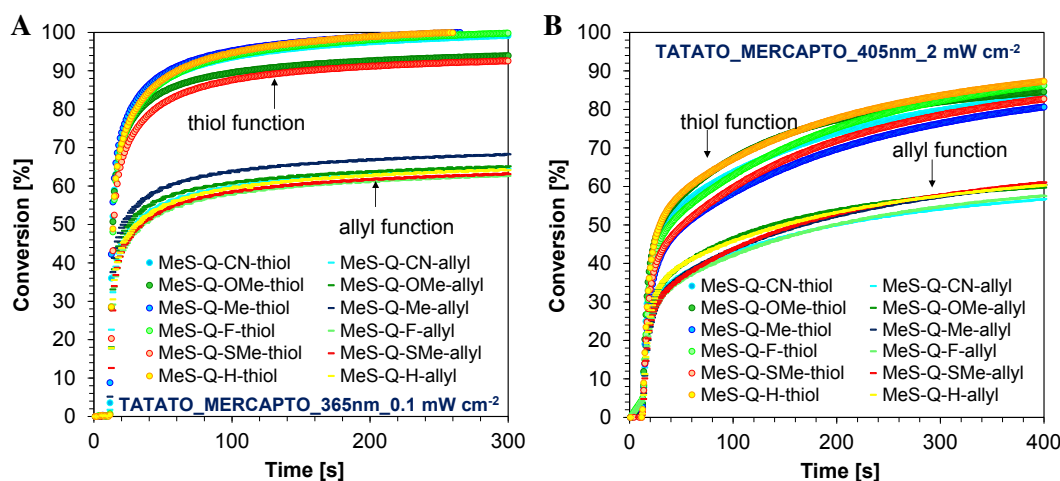


**Fig. 13.** Polymerisation profiles of TATATO/MERCAPTO (50/50% w/w) (thiol and allyl function conversion vs. irradiation time) in the presence of different photoinitiating systems based on 4,4'-dimethyl-diphenyl iodonium hexafluorophosphate (OMNICAT 440, 1%) and 6-(4-methylsulfanylphenyl)-1-phenyl-quinolin-2-one derivatives (0.1%): (A) upon exposure to the LED@365 nm (0.1 mW cm<sup>-2</sup>); (B) upon exposure to the LED@405 nm (2 mW cm<sup>-2</sup>). The irradiation starts at t = 10 s.

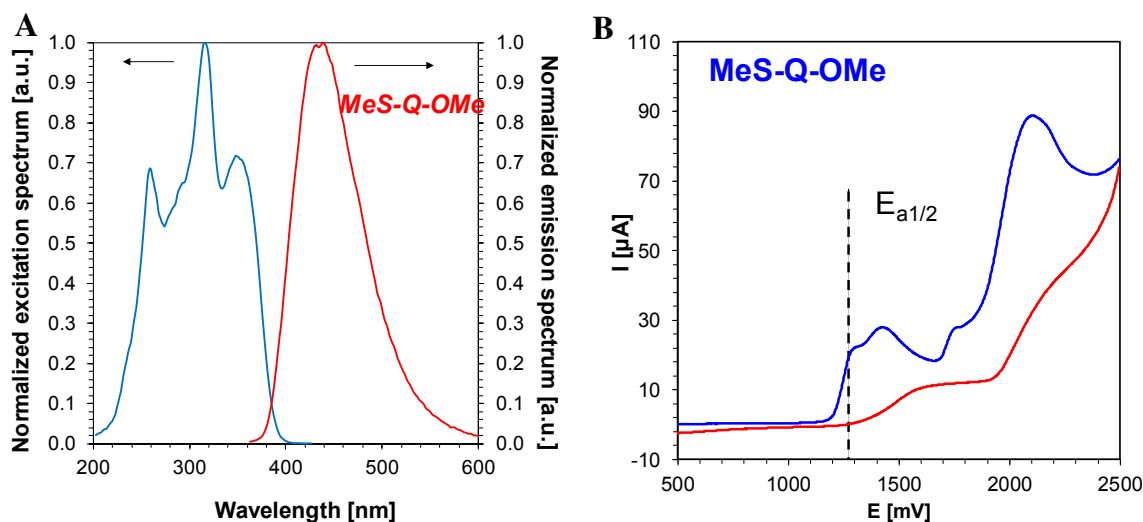


**Fig. 14.** (A) Absorption and fluorescence spectra for the determination of the excited singlet state energy for MeS-Q-OMe derivative; (B) Cyclic voltammogram curves of the MeS-Q-OMe oxidation in acetonitrile.

**Table 5**

Electrochemical and thermodynamical properties of 6-(4-methylsulfanylphenyl)-1-phenyl-quinolin-2-one derivatives.

Fluorescent sensor / Photosensitizer	$E_{ox}^{1/2}$ [mV]	$E_{00(S)}$ [eV]	$\Delta G_{et(S)}$ [eV]	$E_{red}^{1/2}$ [mV]	$E_{00(T)}$ [eV]	$\Delta G_{et(T)}$ [eV]	$K_{SV}$ [M <sup>-1</sup> ]	$\Phi_{et(S)}$
MeS-Q-H	1317	3.20	-1.25	-1968	2.58	-0.63	50.955	0.49
MeS-Q-OMe	1273	3.20	-1.29	-1993	2.59	-0.67	49.190	0.48
MeS-Q-Me	1301	3.21	-1.27	-1985	2.57	-0.63	39.258	0.42
MeS-Q-SMe	1313	3.20	-1.24	-1960	2.58	-0.63	31.901	0.37
MeS-Q-F	1317	3.22	-1.26	-1953	2.58	-0.62	44.961	0.46
MeS-Q-CN	1291	3.19	-1.26	-1858	2.55	-0.64	50.450	0.48

$E_{ox}^{1/2}$  - the electrochemically determined oxidation half-wave potentials (vs. Ag/AgCl) of the photosensitizer (the electron donor).

$E_{red}^{1/2}$  - the electrochemically determined reduction half-wave potentials (vs. Ag/AgCl) of the 4,4'-dimethyl-diphenyl iodonium hexafluorophosphate (OMNICAT 440) (the electron acceptor) -  $E_{red}^{1/2} OMNICAT440 = -0.64$  V vs. SCE (-0.72 V vs. Ag/AgCl) [5,65].

$E_{00}$  - the excitation energy of the co-initiator, which is referred to as singlet excitation energy.

$\Delta G_{et}$  - the enthalpy of free electron transfer (calculated from the Rhema-Weller formula);  $\Phi_{et(S)}$  - the electron transfer quantum yields from the excited singlet state from

the equation:  $\Phi_{et(S)} = \frac{K_{SV}[Q]}{K_{SV}[Q] + 1}$  [Q] = 0.0186 ME<sub>N</sub><sup>+</sup> - scale of polarity [8]  $\lambda_{max-ex}$  - wavelength for the maximum intensity of the excitation spectrum [nm]  $\lambda_{max-fl}$  - wavelengths for the maximum intensity of the emission spectrum [nm]<sup>a</sup> changes in fluorescence intensity expressed as a percentage in relation to the initial value before polymerisation<sup>b</sup> Relative sensitivity  $S_{rel}$  as a reference sensor Coumarin 1 was used.

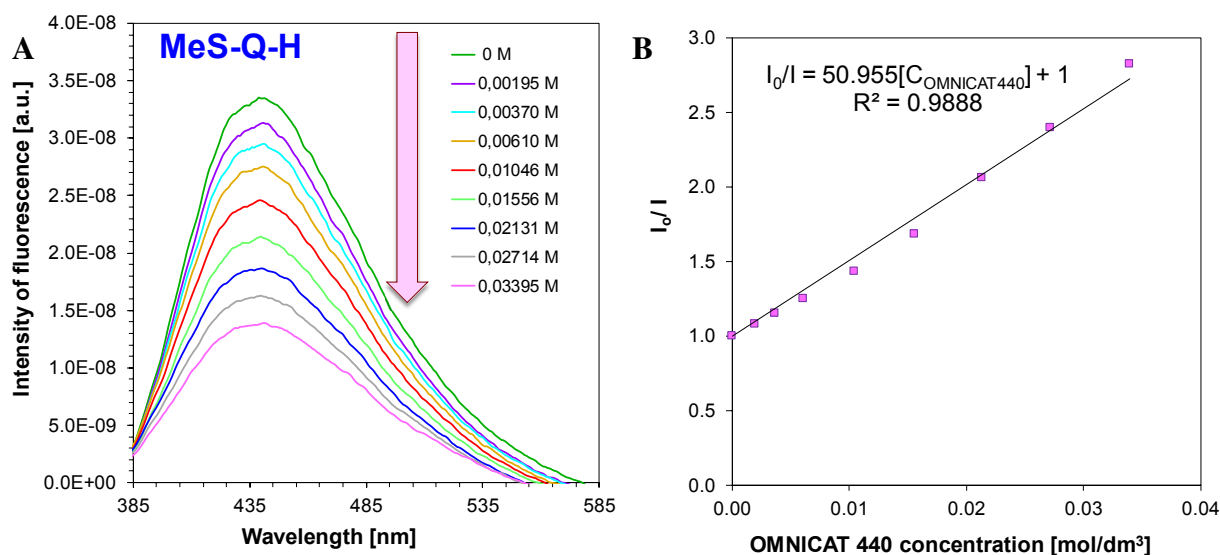


Fig. 15. (A) Fluorescence emission quenching of MeS-Q-H by different concentration of OMNICAT 440 in ACN; concentration [MeS-Q-SMe] =  $1.46 \cdot 10^{-5}$  [mol/dm<sup>3</sup>]; (B) Stern-Volmer treatment for the MeS-Q-H/Iod fluorescence quenching.

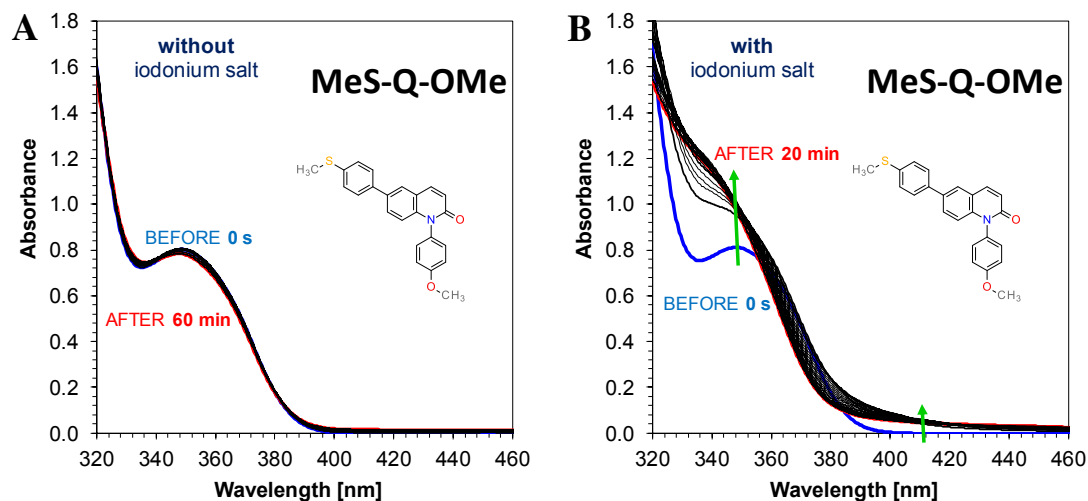


Fig. 16. (A) Photolysis of MeS-Q-OMe (concentration:  $1.62 \cdot 10^{-1}$  [mol/dm<sup>3</sup>]) in ACN under 365 nm (14 mW/cm<sup>2</sup>); (B) Photolysis of MeS-Q-OMe + OMNICAT 440 (concentration:  $1.62 \cdot 10^{-3}$  [mol/dm<sup>3</sup>]) in ACN under 365 nm (14 mW/cm<sup>2</sup>).

S94, S96). Photolysis occurs very quickly and indicates the interaction of 6-(4-methylsulfanylphenyl)-1-phenyl-quinolin-2-one derivatives with the OMNICAT 440 iodonium salt.

#### 4. 3D printing experiment

3D printing experiments with laser diode irradiation 405 nm were carried out in air using the two-component initiating system in the form of the 6-(4-methylsulfanylphenyl)-1-phenyl-quinolin-2-one derivative - MeS-Q-OMe (0.05% w/w)/OMNICAT 440 (1% w/w) (PK pattern) and - MeS-Q-CN (0.05% w/w)/OMNICAT 440 (1% w/w) (MT pattern) and mixtures of CADE/TMPTA monomers in a weight ratio of 1: 1. It is necessary to use these two monomers due to the fact that the TMPTA acrylate monomer provides good print resolution, while the CADE epoxy monomer limits the negative effect of oxygen inhibition. The resolution for two different initiating systems was different. In the case of the initiating system containing the MeS-Q-OMe compound, the resolution of the obtained patterns was high, while in the case of the initiating system containing the MeS-Q-CN compound, the resolution was low. The initiating system containing the MeS-Q-OMe can be used as a

fluorescent label obtained by printing. The obtained patterns were analyzed by microscope, and the patterns are shown in Figs. 17 and 18.

#### 5. Conclusions

New two-component initiating systems consisting of 1,6-diphenyl-quinolin-2-one derivatives and the OMNICAT 440 iodonium initiator are effective in initiating cationic photopolymerisation processes of CADE epoxy and vinyl TEGDVE monomers, free-radical photopolymerisation of TMPTA acrylic monomer as well as thiol-ene photopolymerisation of mixture of monomers: TATATO/MERCAPTO. Nevertheless, the type of built-in substituent for quinolin-1-one chromophore has an impact on the efficiency of initiation, and thus on the quality of the patterns obtained using the 3-D print method. The best system for initiating photopolymerisation processes of all types is a system composed of MeS-Q-OMe, (the compound having a strongly electron-donor substituent) and the OMNICAT 440 iodonium salt. Using this initiating system, 3-D prints with very good resolution are obtained.

Moreover, the developed compounds are also suitable for the role of molecular probes for monitoring the kinetics of both radical and thiol-en

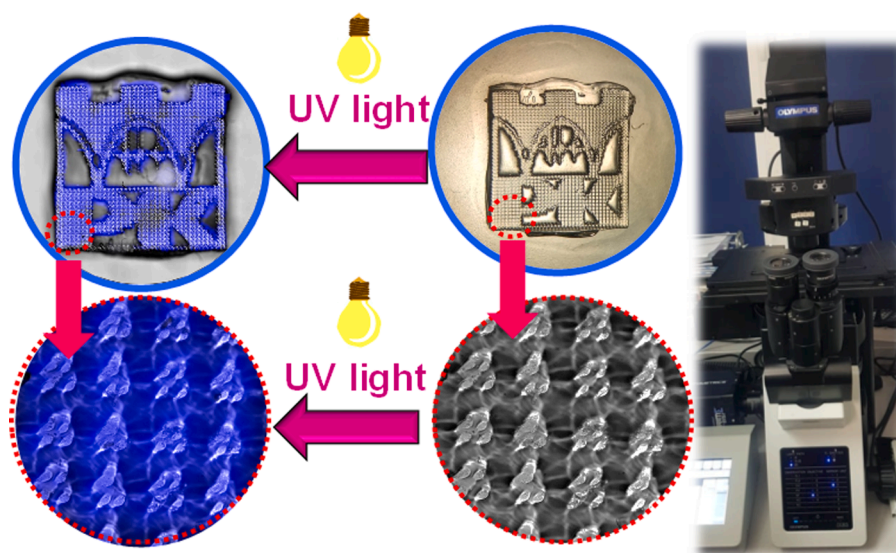


**Fig. 17.** The patterns (logo of the Cracow University of Technology) obtained after the 3D printing experiment based on formulations MeS-Q-OMe (0.05% w/w)/OMNICAT 440 (1.0% w/w)/TMPTA/CADE (1 : 1 w/w): (A) Characterization of the 3D patterns by fluorescent microscopy; (B) Characterization of the 3D patterns by numerical optical microscopy.

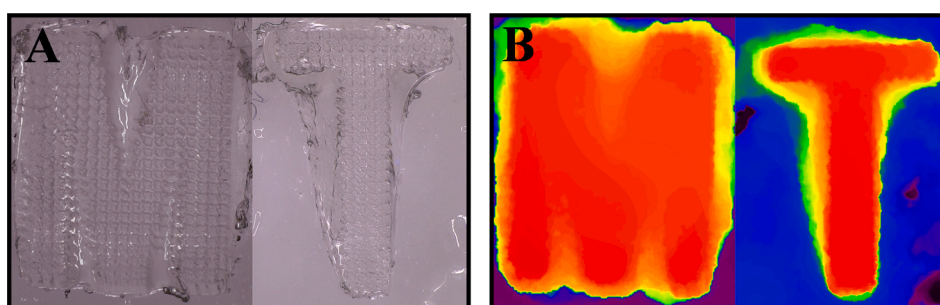


**Fig. 18.** The patterns (MT LETTERS) obtained after the 3D printing experiment based on formulations MeS-Q-CN (0.05% w/w)/OMNICAT 440 (1.0% w/w)/TMPTA/CADE (1 : 1 w/w): Characterization of the 3D patterns by numerical optical microscopy.

photopolymerisation processes. However, in this case the highest sensitivity was obtained for a compound having a strongly electron withdrawing substituent  $-CN$  (MeS-Q-CN compound).

#### CRediT authorship contribution statement

**Monika Topa:** Conceptualization, Methodology, Validation, Formal analysis, Investigation, Data curation, Writing - original draft, Visualization. **Filip Petko:** Investigation. **Mariusz Galek:** Investigation. **Magdalena Jankowska:** Formal analysis, Investigation. **Roman Popielarz:** Software. **Joanna Ortyl:** Conceptualization, Methodology, Validation, Resources, Data curation, Writing - review & editing, Visualization, Supervision, Project administration, Funding acquisition.

#### Declaration of Competing Interest

The authors declare that they have no known competing financial interests or personal relationships that could have appeared to influence the work reported in this paper.

#### Acknowledgment

This research was funded by the Foundation for Polish Science (Warsaw, Poland) grant number REINTEGRATION/2016-1/4 (POIR.04.04.00-00-1E42/16-00) "Synthesis and photochemistry/photophysics studies of the intelligent luminescent molecular sensors for

selective detection in biochemistry and chemistry."

The authors are also grateful to the Foundation for Polish Science (Warsaw, Poland) TEAM TECH project Grant No. TEAM TECH/2016-2/15 (POIR.04.04.00-00-204B/16-00) for financing the purchase of 3D printing equipment and to the National Science Centre – Project SONATA [Grant No. UMO-2012/07/D/ST5/02300, 2012] for financing the purchase of steady-state fluorescence spectrofluorometer and real-time FT-IR spectrometer. The computational procedures were done by using open infrastructure resources PLGrid Infrastructure.

The authors are also grateful to the Olympus Company and Mr Mateusz Pernak for presentation the optical microscope DSX1000 and possibility made an observation of patterns written during the photopolymerisation of composition under air using new bimolecular photo-initiating systems by this type of microscope. The authors are also grateful to the OLYMPUS Poland (High End Life Science Systems) and Dr Wojciech Brutkowsky for presentation the on an inverted fluorescence microscope Olympus IX83 and possibility made an observation of patterns written during the photopolymerisation of composition under air using new bimolecular photoinitiating systems by this type of microscope.

#### Appendix A. Supplementary material

Supplementary data to this article can be found online at <https://doi.org/10.1016/j.eurpolymj.2021.110612>.

## References

- [1] C. Mendes-Felipe, J. Oliveira, I. Etxebarria, J.L. Vilas-Vilela, S. Lanceros-Mendez, State-of-the-Art and Future Challenges of UV Curable Polymer-Based Smart Materials for Printing Technologies, *Adv. Mater. Technol.* 4 (2019) 1800618, <https://doi.org/10.1002/admt.201800618>.
- [2] J. Shao, Y. Huang, Q. Fan, Visible light initiating systems for photopolymerization: Status, development and challenges, *Polym. Chem.* 5 (2014) 4195–4210, <https://doi.org/10.1039/c4py00072b>.
- [3] N. Corrigan, J. Yeow, P. Judzewitsch, J. Xu, C. Boyer, Seeing the Light: Advancing Materials Chemistry through Photopolymerization, *Angew. Chemie Int. Ed.* 58 (2019) 5170–5189, <https://doi.org/10.1002/anie.201805473>.
- [4] A. Vitale, G. Trusiano, R. Bongiovanni, UV-Curing of Adhesives: A Critical Review, in: *Prog. Adhes. Adhes.*, John Wiley & Sons, Inc., Hoboken, NJ, USA, 2018: pp. 101–154. <https://doi.org/10.1002/9781119526445.ch4>.
- [5] B. Strehmel, S. Ernst, K. Reiner, D. Keil, H. Lindauer, H. Baumann, Application of nir-photopolymers in the graphic industry: From physical chemistry to lithographic applications, *Zeitschrift Fur Phys. Chemie.* 228 (2014) 129–153, <https://doi.org/10.1515/zpch-2014-0451>.
- [6] P.A.M. Steeman, A.A. Dias, D. Wienke, T. Zwartkruis, Polymerization and network formation of UV-curable systems monitored by hyphenated real-time dynamic mechanical analysis and near-infrared spectroscopy, *Macromolecules.* 37 (2004) 7001–7007, <https://doi.org/10.1021/ma049366c>.
- [7] D.A. Abu-Elenain, S.H. Lewis, J.W. Stansbury, Property evolution during vitrification of dimethacrylate photopolymer networks, *Dent. Mater.* 29 (2013) 1173–1181, <https://doi.org/10.1016/j.dental.2013.09.002>.
- [8] J.W. Stansbury, M. Trujillo-Lemon, H. Lu, X. Ding, Y. Lin, J. Ge, Conversion-dependent shrinkage stress and strain in dental resins and composites, *Dent. Mater.* 21 (2005) 56–67, <https://doi.org/10.1016/j.dental.2004.10.006>.
- [9] J. Li, S. Li, Y. Li, R. Li, J. Nie, X. Zhu, In situ monitoring of photopolymerization by photoinitiator with luminescence characteristics, *J. Photochem. Photobiol. A Chem.* 389 (2020), 112225, <https://doi.org/10.1016/j.jphotochem.2019.112225>.
- [10] J. Xu, Y. Jiang, T. Zhang, Y. Dai, D. Yang, F. Qiu, Z. Yu, P. Yang, Synthesis of UV-curing waterborne polyurethane-acrylate coating and its photopolymerization kinetics using FT-IR and photo-DSC methods, *Prog. Org. Coatings.* 122 (2018) 10–18, <https://doi.org/10.1016/j.porgcoat.2018.05.008>.
- [11] P. Bosch, A. Fernández-Arizepe, F. Catalina, J.L. Mateo, C. Peinado, New fluorescent probes for monitoring polymerization reactions: Photocuring of acrylic adhesives, *Macromol. Chem. Phys.* 203 (2002) 336–345, [https://doi.org/10.1002/1522-3935\(20020101\)203:2<336::AID-MACP336>3.0.CO;2-B](https://doi.org/10.1002/1522-3935(20020101)203:2<336::AID-MACP336>3.0.CO;2-B).
- [12] T. Scherzer, VUV-induced photopolymerization of acrylates, *Macromol. Chem. Phys.* 213 (2012) 324–334, <https://doi.org/10.1002/macp.201100485>.
- [13] D.B. Yang, Kinetic studies of photopolymerization using real time FT-IR spectroscopy, *J. Polym. Sci. Part A Polym. Chem.* 31 (1993) 199–208, <https://doi.org/10.1002/pola.1993.080310124>.
- [14] H.K. Yang, M.S. Kim, S.W. Kang, K.S. Kim, K.S. Lee, S.H. Park, D.Y. Yang, H. J. Kong, H.B. Sun, S. Kawata, P. Fleitz, Recent progress of lithographic microfabrication by the TPA-induced photopolymerization, *J. Photopolym. Sci. Technol.* 17 (2004) 385–392, <https://doi.org/10.2494/photopolym.17.385>.
- [15] P. Xiao, J. Zhang, F. Dumur, M.A. Tehfe, F. Morlet-Savary, B. Graff, D. Gignès, J. P. Fouassier, J. Lalevée, Visible light sensitive photoinitiating systems: Recent progress in cationic and radical photopolymerization reactions under soft conditions, *Prog. Polym. Sci.* 41 (2015) 32–66, <https://doi.org/10.1016/j.progpolymsci.2014.09.001>.
- [16] A. Wagner, M. Mühlberger, C. Paulik, Photoinitiator-free photopolymerization of acrylate-bismaleimide mixtures and their application for inkjet printing, *J. Appl. Polym. Sci.* 136 (2019) 1–9, <https://doi.org/10.1002/app.47789>.
- [17] P. Cakir Hatir, G. Cayli, Environmentally friendly synthesis and photopolymerization of acrylated methyl ricinoleate for biomedical applications, *J. Appl. Polym. Sci.* 136 (2019) 1–8, <https://doi.org/10.1002/app.47969>.
- [18] D.M. Djordjevic, S.T. Cirkovic, D.S. Mandic, Biomedical applications, *Magn. Ferroelectr. Multiferroic Met. Oxides.* (2018) 411–430, <https://doi.org/10.1016/B978-0-12-811180-2.00020-7>.
- [19] G.A. Appuhamillage, N. Chartrain, V. Meenakshisundaram, K.D. Feller, C. B. Williams, T.E. Long, 110th Anniversary: Vat Photopolymerization-Based Additive Manufacturing: Current Trends and Future Directions in Materials Design, *Ind. Eng. Chem. Res.* 58 (2019) 15109–15118, <https://doi.org/10.1021/acs.iecr.9b02679>.
- [20] M. Pagac, J. Hajnys, Q.P. Ma, L. Jancar, J. Jansa, P. Stefek, J. Mesicek, A review of vat photopolymerization technology: Materials, applications, challenges, and future trends of 3d printing, *Polymers (Basel).* 13 (2021) 1–20, <https://doi.org/10.3390/polym13040598>.
- [21] G. Diptanshu, C. Miao, Ma, Vat photopolymerization 3D printing of ceramics: Effects of fine powder, *Manuf. Lett.* 21 (2019) 20–23, <https://doi.org/10.1016/j.mflet.2019.07.001>.
- [22] W.N. Nkeuwa, B. Riedl, V. Landry, UV-cured clay/based nanocomposite topcoats for wood furniture: Part I: Morphological study, water vapor transmission rate and optical clarity, *Prog. Org. Coatings.* 77 (2014) 1–11, <https://doi.org/10.1016/j.porgcoat.2013.03.021>.
- [23] A. Shibuya, K. Kunita, S. Koizumi, High sensitive photopolymerization initiator system using violet laser and its application to photopolymer CTP plate, *J. Photopolym. Sci. Technol.* 26 (2013) 249–254, <https://doi.org/10.2494/photopolym.26.249>.
- [24] V. Maurin, C. Croutxé-Barghorn, X. Allonas, Photopolymerization process of UV powders. Characterization of coating properties, *Prog. Org. Coatings.* 73 (2012) 250–256, <https://doi.org/10.1016/j.porgcoat.2011.11.010>.
- [25] A. Javadi, H.S. Mehr, M. Sobani, M.D. Soucek, Cure-on-command technology: A review of the current state of the art, *Prog. Org. Coatings.* 100 (2016) 2–31, <https://doi.org/10.1016/j.porgcoat.2016.02.014>.
- [26] S. Chung, S. Park, I. Lee, H. Jeong, D. Cho, A study on microreplication of real 3D-shape structures using elastomeric mold: From pure epoxy to composite based on epoxy, *Int. J. Mach. Tools Manuf.* 44 (2004) 147–154, <https://doi.org/10.1016/j.ijmactools.2003.10.017>.
- [27] S. Schoerpf, Y. Catel, N. Moszner, C. Gorsche, R. Liska, Enhanced reduction of polymerization-induced shrinkage stress: Via combination of radical ring opening and addition fragmentation chain transfer, *Polym. Chem.* 10 (2019) 1357–1366, <https://doi.org/10.1039/c8py01540f>.
- [28] Z. Zhao, J. Wu, X. Mu, H. Chen, H.J. Qi, D. Fang, Origami by frontal photopolymerization, *Sci. Adv.* 3 (2017) 1–8, <https://doi.org/10.1126/sciadv.1602326>.
- [29] A. Accardo, R. Courson, R. Riesco, V. Raimbault, L. Malaquin, Direct laser fabrication of meso-scale 2D and 3D architectures with micrometric feature resolution, *Addit. Manuf.* 22 (2018) 440–446, <https://doi.org/10.1016/j.addma.2018.04.027>.
- [30] A. Vitale, M. Sangermano, R. Bongiovanni, P. Burtscher, N. Moszner, Visible light curable restorative composites for dental applications based on epoxy monomer, *Materials (Basel).* 7 (2014) 554–562, <https://doi.org/10.3390/ma7010554>.
- [31] M. Topa, J. Ortyl, Moving towards a finer way of light-cured resin-based restorative dental materials: Recent advances in photoinitiating systems based on iodonium salts, *Materials (Basel).* 13 (2020) 4093, <https://doi.org/10.3390/ma13184093>.
- [32] A.A. Pérez-Mondragón, C.E. Cuevas-Suárez, J.A. González-López, N. Trejo-Carbajal, A.M. Herrera-González, Evaluation of new cointiators of camphorquinone useful in the radical photopolymerization of dental monomers, *J. Photochem. Photobiol. A Chem.* 403 (2020), 112844, <https://doi.org/10.1016/j.jphotochem.2020.112844>.
- [33] N. Monteiro, G. Thirivikraman, A. Athirasala, A. Tahayeri, C.M. França, J. L. Ferracane, L.E. Bertassoni, Photopolymerization of cell-laden gelatin methacryloyl hydrogels using a dental curing light for regenerative dentistry, *Dent. Mater.* 34 (2018) 389–399, <https://doi.org/10.1016/j.dental.2017.11.020>.
- [34] E. Hola, M. Topa, A. Chachaj-Brekiesz, M. Pilch, P. Fiedor, M. Galek, J. Ortyl, New, highly versatile bimolecular photoinitiating systems for free-radical, cationic and thiol-ene photopolymerization processes under low light intensity UV and visible LEDs for 3D printing application, *RSC Adv.* 10 (2020) 7509–7522, <https://doi.org/10.1039/c9ra10212d>.
- [35] A. Baralle, P. Garra, F. Morlet-Savary, C. Dietlin, J.P. Fouassier, J. Lalevée, Polymeric Iodonium Salts to Trigger Free Radical Photopolymerization, *Macromol. Rapid Commun.* 41 (2020) 1900644, <https://doi.org/10.1002/marc.201900644>.
- [36] P. Fiedor, M. Pilch, P. Szymaszek, A. Chachaj-Brekiesz, M. Galek, J. Ortyl, Photochemical study of a new bimolecular photoinitiating system for vat photopolymerization 3D printing techniques under visible light, *Catalysts.* 10 (2020) 284, <https://doi.org/10.3390/catal10030284>.
- [37] A. Bagheri, J. Jin, Photopolymerization in 3D Printing, *ACS Appl. Polym. Mater.* 1 (2019) 593–611, <https://doi.org/10.1021/acscapm.8b00165>.
- [38] J. Zhang, P. Xiao, 3D printing of photopolymers, *Polym. Chem.* 9 (2018) 1530–1540, <https://doi.org/10.1039/c8py00157j>.
- [39] J. Liu, K. Zhu, T. Jiao, R. Xing, W. Hong, L. Zhang, Q. Zhang, Q. Peng, Preparation of graphene oxide-polymer composite hydrogels via thiol-ene photopolymerization as efficient dye adsorbents for wastewater treatment, *Colloids Surf. A Physicochem. Eng. Asp.* 529 (2017) 668–676, <https://doi.org/10.1016/j.colsurfa.2017.06.050>.
- [40] J. Su, Y. Yang, Z. Chen, J. Zhou, X. Liu, Y. Fang, Y. Cui, Preparation and performance of thermosensitive poly(N-isopropylacrylamide) hydrogels by frontal photopolymerization, *Polym. Int.* 68 (2019) 1673–1680, <https://doi.org/10.1002/pi.5868>.
- [41] D. Pieniak, A.M. Niewczas, M. Walczak, J. Zamościńska, Influence of photopolymerization parameters on the mechanical properties of polymer-ceramic composites applied in the conservative dentistry, *Acta Bioeng. Biomech.* 16 (2014) 29–35, <https://doi.org/10.5277/abbi140304>.
- [42] W. Kasprzyk, S. Bednarz, D. Bogdał, G.A. Ameer, T. Świergosz, Cyclodextrin-modified poly(octamethylene citrate) polymers towards enhanced sorption properties, *Soft Matter.* 16 (2020) 3311–3318, <https://doi.org/10.1039/C9SM02075F>.
- [43] J.P. Fisher, D. Dean, P.S. Engel, A.G. Mikos, Photoinitiated polymerization of biomaterials, *Annu. Rev. Mater. Res.* 31 (2001) 171–181, <https://doi.org/10.1146/annurev.matsci.31.1.171>.
- [44] X. Jia, X. Jiang, R. Liu, J. Yin, Facile approach to patterned binary polymer brush through photolithography and surface-initiated photopolymerization, *ACS Appl. Mater. Interf.* 2 (2010) 1200–1205, <https://doi.org/10.1021/am100035d>.
- [45] A. Espanet, G. Dos Santos, C. Ecoffet, D.J. Lounnot, Photopolymerization by evanescent waves: Characterization of photopolymerizable formulation for photolithography with nanometric resolution, *Appl. Surf. Sci.* 138–139 (1999) 87–92, [https://doi.org/10.1016/S0169-4332\(98\)00388-2](https://doi.org/10.1016/S0169-4332(98)00388-2).
- [46] A. Vitale, M. Quaglio, M. Cocuzza, C.F. Pirri, R. Bongiovanni, Photopolymerization of a perfluoropolyether oligomer and photolithographic processes for the fabrication of microfluidic devices, *Eur. Polym. J.* 48 (2012) 1118–1126, <https://doi.org/10.1016/j.eurpolymj.2012.03.016>.
- [47] A. Al Mousawi, C. Dietlin, B. Graff, F. Morlet-Savary, J. Toufaily, T. Hamieh, J.P. Fouassier, A. Chachaj-Brekiesz, J. Ortyl, J. Lalevée, Meta-Terphenyl Derivative/Iodonium Salt/9H-Carbazole-9-ethanol Photoinitiating Systems for Free Radical Promoted Cationic Polymerization upon Visible Lights, *Macromol. Chem. Phys.* 217 (2016) 1955–1965, <https://doi.org/10.1002/macp.201600224>.

- [48] J. Kabatc, J. Ortyl, K. Kostrzewska, New kinetic and mechanistic aspects of photosensitization of iodonium salts in photopolymerization of acrylates, *RSC Adv.* 7 (2017) 41619–41629, <https://doi.org/10.1039/c7ra05978g>.
- [49] K. Kostrzewska, J. Ortyl, R. Dobosz, J. Kabatc, Squarylium dye and onium salts as highly sensitive photoradical generators for blue light, *Polym. Chem.* 8 (2017) 3464–3474, <https://doi.org/10.1039/c7py00621g>.
- [50] J. Ortyl, P. Milart, R. Popielarz, Applicability of aminophthalimide probes for monitoring and acceleration of cationic photopolymerization of epoxides, *Polym. Test.* 32 (2013) 708–715, <https://doi.org/10.1016/j.polymertesting.2013.03.009>.
- [51] H. Chen, G. Noirbent, Y. Zhang, K. Sun, S. Liu, D. Brunel, D. Gimes, B. Graff, F. Morlet-Savary, P. Xiao, F. Dumur, J. Lalevée, Photopolymerization and 3D/4D applications using newly developed dyes: Search around the natural chalcone scaffold in photoinitiating systems, *Dye. Pigment.* 188 (2021), 109213, <https://doi.org/10.1016/j.dyepig.2021.109213>.
- [52] K. Lee, N. Corrigan, C. Boyer, Rapid High-Resolution 3D Printing and Surface Functionalization via Type I Photoinitiated RAFT Polymerization, *Angew. Chemie - Int. Ed.* 60 (2021) 8839–8850, <https://doi.org/10.1002/anie.202016523>.
- [53] Y. Zhu, J. Pi, Y. Zhang, D. Xu, Y. Yagci, R. Liu, A new anthraquinone derivative as a near UV and visible light photoinitiator for free-radical, thiol-ene and cationic polymerizations, *Polym. Chem.* 12 (2021) 3299–3306, <https://doi.org/10.1039/d1py00347j>.
- [54] M. Topa, F. Petko, M. Galek, K. Machowski, M. Pilch, P. Szymaszek, J. Ortyl, Applicability of 1,6-Diphenylquinolin-2-one derivatives as fluorescent sensors for monitoring the progress of photopolymerisation processes and as photosensitisers for bimolecular photoinitiating systems, *Polymers (Basel)*. 11 (2019) 1756, <https://doi.org/10.3390/polym11111756>.
- [55] J. Ortyl, J. Wilamowski, P. Milart, M. Galek, R. Popielarz, Relative sensitization efficiency of fluorescent probes/sensitizers for monitoring and acceleration of cationic photopolymerization of monomers, *Polym. Test.* 48 (2015) 151–159, <https://doi.org/10.1016/j.polymertesting.2015.10.006>.
- [56] D. Nowak, J. Ortyl, I. Kamińska-Borek, K. Kukula, M. Topa, R. Popielarz, Photopolymerization of hybrid monomers, Part II: Determination of relative quantum efficiency of selected photoinitiators in cationic and free-radical polymerization of hybrid monomers, *Polym. Test.* 67 (2018) 144–150, <https://doi.org/10.1016/j.polymertesting.2018.02.025>.
- [57] I. Kamińska, J. Ortyl, R. Popielarz, Applicability of quinolizino-coumarins for monitoring free radical photopolymerization by fluorescence spectroscopy, *Polym. Test.* 42 (2015) 99–107, <https://doi.org/10.1016/j.polymertesting.2014.12.013>.
- [58] J. Ortyl, M. Galica, R. Popielarz, D. Bogdal, Application of a carbazole derivative as a spectroscopic fluorescent probe for real time monitoring of cationic photopolymerization, *Polish J. Chem. Technol.* 16 (2014) 75–80, <https://doi.org/10.2478/pjct-2014-0013>.
- [59] J. Ortyl, M. Topa, I. Kamińska-Borek, R. Popielarz, Mechanism of interaction of aminocoumarins with reaction medium during cationic photopolymerization of triethylene glycol divinyl ether, *Eur. Polym. J.* 116 (2019) 45–55, <https://doi.org/10.1016/j.eurpolymj.2019.03.060>.
- [60] M. Topa, J. Ortyl, A. Chachaj-Brekiesz, I. Kamińska-Borek, M. Pilch, R. Popielarz, Applicability of samarium(III) complexes for the role of luminescent molecular sensors for monitoring progress of photopolymerization processes and control of the thickness of polymer coatings, *Spectrochim. Acta - Part A Mol. Biomol. Spectrosc.* 199 (2018) 430–440, <https://doi.org/10.1016/j.saa.2018.03.050>.
- [61] W.E. Ernst, J. Kändler, S. Kindt, T. Törring, Electric dipole moment of  $\text{SrF X}^{2\Sigma^+}$  from high-precision stark effect measurements, *Chem. Phys. Lett.* 113 (1985) 351–354, [https://doi.org/10.1016/0009-2614\(85\)80379-1](https://doi.org/10.1016/0009-2614(85)80379-1).
- [62] C. Reichardt, Solvatochromic dyes as solvent polarity indicators, *Chem. Rev.* 94 (1994) 2319–2358, <https://doi.org/10.1021/cr00032a005>.
- [63] S. Medel, P. Bosch, I. Grabchev, P.K. Shah, J. Liu, A. Aguirre-Soto, J.W. Stansbury, Simultaneous measurement of fluorescence, conversion and physical/mechanical properties for monitoring bulk and localized photopolymerization reactions in heterogeneous systems, *RSC Adv.* 6 (2016) 41275–41286, <https://doi.org/10.1039/c6ra06341a>.
- [64] S. Bayou, M. Mouzali, F. Aloui, L. Lecamp, P. Lebaudy, Simulation of conversion profiles inside a thick dental material photopolymerized in the presence of nanofillers, *Polym. J.* 45 (2013) 863–870, <https://doi.org/10.1038/pj.2012.226>.
- [65] P.P. Romańczyk, S.S. Kurek, The Reduction Potential of Diphenyliodonium polymerisation photoinitiator Is Not  $-0.2$  V vs. SCE. a computational study, *Electrochim. Acta.* 255 (2017) 482–485, <https://doi.org/10.1016/j.electacta.2017.09.166>.